RESEARCH ARTICLE

Agent-based model demonstrates the impact of nonlinear, complex interactions between cytokines on muscle regeneration

Megan Haase[1], Tien Comlekoglu[1], Alexa Petrucciani[2], Shayn M Peirce[1], Silvia S Blemker[1]*

[1]University of Virginia, Charlottesville, United States; [2]Purdue University, West Lafayette, United States

Abstract Muscle regeneration is a complex process due to dynamic and multiscale biochemical and cellular interactions, making it difficult to identify microenvironmental conditions that are beneficial to muscle recovery from injury using experimental approaches alone. To understand the degree to which individual cellular behaviors impact endogenous mechanisms of muscle recovery, we developed an agent-based model (ABM) using the Cellular-Potts framework to simulate the dynamic microenvironment of a cross-section of murine skeletal muscle tissue. We referenced more than 100 published studies to define over 100 parameters and rules that dictate the behavior of muscle fibers, satellite stem cells (SSCs), fibroblasts, neutrophils, macrophages, microvessels, and lymphatic vessels, as well as their interactions with each other and the microenvironment. We utilized parameter density estimation to calibrate the model to temporal biological datasets describing cross-sectional area (CSA) recovery, SSC, and fibroblast cell counts at multiple timepoints following injury. The calibrated model was validated by comparison of other model outputs (macrophage, neutrophil, and capillaries counts) to experimental observations. Predictions for eight model perturbations that varied cell or cytokine input conditions were compared to published experimental studies to validate model predictive capabilities. We used Latin hypercube sampling and partial rank correlation coefficient to identify in silico perturbations of cytokine diffusion coefficients and decay rates to enhance CSA recovery. This analysis suggests that combined alterations of specific cytokine decay and diffusion parameters result in greater fibroblast and SSC proliferation compared to individual perturbations with a 13% increase in CSA recovery compared to unaltered regeneration at 28 days. These results enable guided development of therapeutic strategies that similarly alter muscle physiology (i.e. converting extracellular matrix [ECM]-bound cytokines into freely diffusible forms as studied in cancer therapeutics or delivery of exogenous cytokines) during regeneration to enhance muscle recovery after injury.

eLife assessment

This is so-far the most comprehensive, spatially resolved in 2D, dynamical, multicellular model of murine muscle regeneration after injury. The work is an attempt to combine many contributors to muscle regeneration into one coherent calibrated framework. The presented analysis is **solid** and the model has the potential to be a very **valuable** tool in the areas of tissue morphogenesis, regenerative therapies, quantitative modeling and simulation.

***For correspondence:** ssblemker@virginia.edu

Competing interest: The authors declare that no competing interests exist.

Funding: See page 22

Preprint posted
16 August 2023
Sent for Review
09 September 2023
Reviewed preprint posted
08 January 2024
Reviewed preprint revised
01 May 2024
Version of Record published
03 June 2024

Reviewing Editor: Frederik Graw, Friedrich-Alexander-University Erlangen-Nürnberg, Germany

Introduction

Skeletal muscle injuries account for more than 30% of all injuries and are one of the most common complaints in orthopedics (***Quintero et al., 2009***; ***Barroso and Thiele, 2011***; ***Valle, 2011***). The standard treatment for muscle injuries is limited mostly to rest, ice, compression, elevation, anti-inflammatory drugs, and immobilization (***Quintero et al., 2009***). These treatments lack a firm scientific basis and have varied outcomes, some resulting in incomplete functional recovery, formation of scar tissue, and high injury recurrence rates (***Järvinen et al., 2007***; ***Huard et al., 2022***). Our fundamental understanding of the individual cellular and subcellular behaviors of muscle cells has advanced and made it clear that interactions between cells and their microenvironment is critical for healthy regeneration. These interactions are dynamic, involve feedback mechanisms, and lead to complex emergent phenomena; therefore, there are numerous possible interventions that could enhance muscle regeneration.

Muscle regeneration requires an abundance of cells and cytokines to interact in a highly coordinated mechanism involving five interrelated cascading phases including degeneration, inflammation, regeneration, remodeling, and functional recovery (***Forcina et al., 2020***). Following an acute muscle injury, there is a time-dependent recruitment of neutrophils, monocytes, and macrophages to remove necrotic tissue and release factors that regulate fibroblast behavior and SSC activation, proliferation, and division (***Howard et al., 2020***). Following initial inflammatory response, fibroblasts and SSCs activate and proliferate with the macrophages shifting from their pro- to anti-inflammatory phenotype. In healthy muscle, this process would be followed by remodeling of the muscle where the fibroblasts apoptose and SSCs differentiate and fuse to repair the myofibers (***Westman et al., 2021***). Each cell involved in this process secretes cytokines that help regulate cell recruitment and chemotaxes to modulate the dynamics of the recovery. It has also been shown that the molecular events implicated in angiogenesis occur at early stages of muscle regeneration to restore microvascular networks that are crucial for successful muscle recovery (***Wagatsuma, 2007***).

There are numerous cytokines involved in muscle regeneration, many of which have been individually studied to examine their influence on muscle regeneration (***Chen et al., 2015***). These cytokines play key roles in dictating cell behaviors and are major drivers of the regeneration cascade (***Husmann et al., 1996***). The dynamics of these cytokines control many aspects of the microenvironment and altering their properties to optimize treatments has been proposed in a variety of settings (***Itoh, 2022***). Testing alterations in cytokine dynamics experimentally has proven to be complex and expensive due to difficulties in cytokine identification and quantification as well as confounding factors due to pleiotropic activities of cytokines and interactions with soluble receptors (***Ciano-Petersen et al., 2022***). These challenges make it difficult to holistically test different diffusion and decay properties for numerous cytokines (***Ferrara, 2010***). However, if we could better understand the synergistic effects of alteration in cytokines, we could design a more effective therapy for treating muscle injury.

There are over a million possible combinations of cytokine alterations, making it unrealistic to study all combinations with experiments alone. For this reason, an in silico approach is needed to fully explore the possible treatment landscape and make predictions on potential targets to enhance muscle recovery. Over the last several years, agent-based models (ABMs) of muscle regeneration have been developed to study muscle regeneration in a variety of applications (***Westman et al., 2021***; ***Virgilio et al., 2018***; ***Martin et al., 2016***; ***Khuu et al., 2021***; ***Khuu et al., 2023***; ***Virgilio et al., 2021***). These models were foundational for exploring the role of SSCs in a variety of muscle milieus (***Westman et al., 2021***; ***Virgilio et al., 2018***; ***Khuu et al., 2021***) and for demonstrating how ABMs can be used to simulate therapeutic interventions (***Martin et al., 2016***). However, previous models employed simplistic, non-spatial representations of cytokine behaviors and properties, which limited their ability to recapitulate cytokine alterations such as injection of transforming growth factor beta (TGF-β) (***Virgilio et al., 2021***). Furthermore, these prior models did not include microvessel adaptations and dynamic extracellular matrix (ECM) properties which are crucial for understanding the altered microenvironmental state following muscle injury. These critical limitations must be addressed in order for ABMs of muscle regeneration to provide meaningful insights into treatments for muscle injury.

The goals of this work were to: (1) develop an ABM of muscle regeneration that includes cellular and cytokine spatial dynamics as well as the microvascular environment, (2) calibrate the model to capture cell behaviors from published experimental studies, (3) validate model outcomes by comparison with

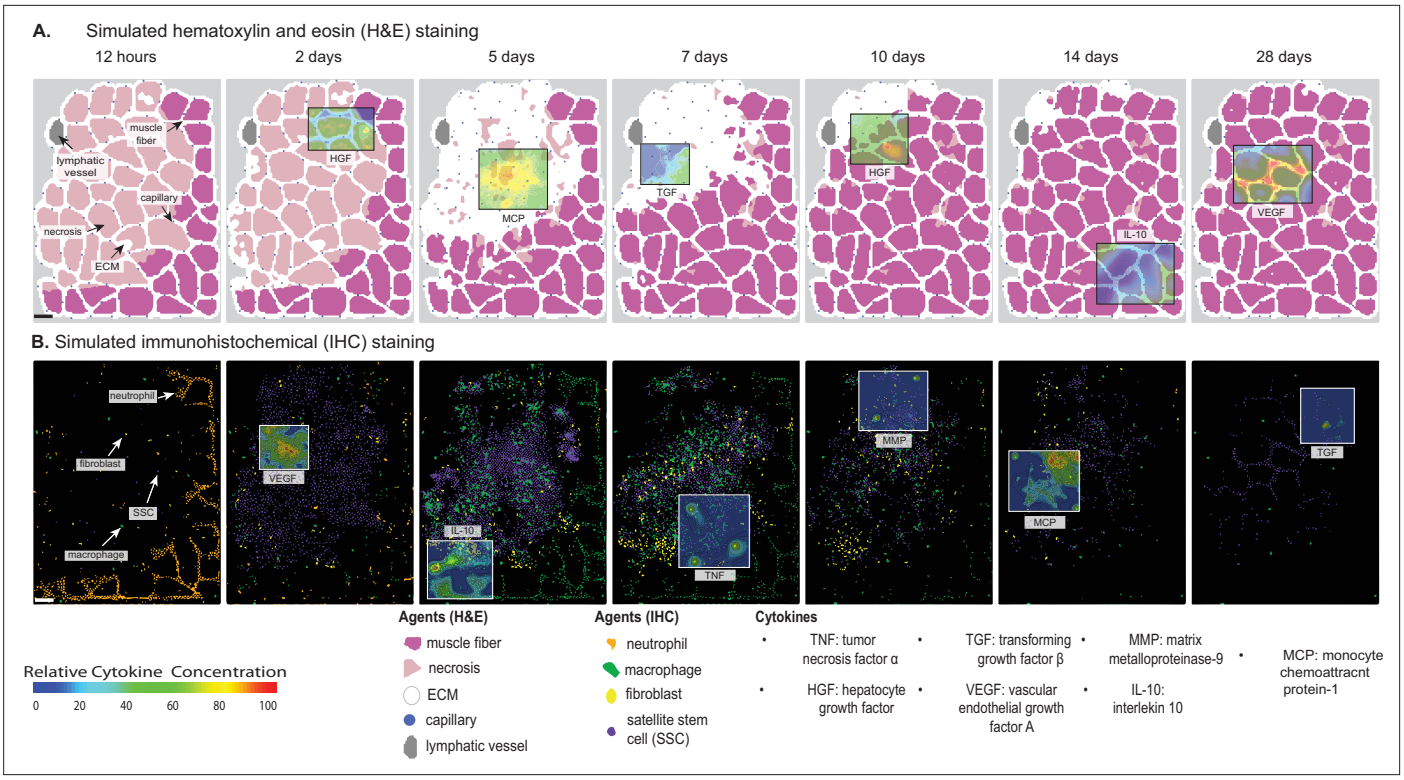

Figure 1. Overview of agent-based model (ABM) simulation of muscle regeneration following an acute injury. (**A**) Simulated cross-sections of a muscle fascicle that was initially defined by spatial geometry from a histology image. Muscle injury was simulated by replacing a section of the healthy fibers with necrotic elements. In response to the injury, a variety of factors are secreted in the microenvironment which impacts the behavior of the cells. The colors correspond with those typically seen in H&E staining. (**B**) ABM screen captures show the spatial locations of the cells throughout the 28-day simulation. The agent colors were matched to those typically seen in IHC-stained muscle sections. Scale bar: 50 μm.

The online version of this article includes the following figure supplement(s) for figure 1:

Figure supplement 1. Overview of agent-based model (ABM) simulation with different initial histology configuration.

multiple published experimental studies, (4) conduct in silico experiments to predict how altering cytokine dynamics impacts muscle regeneration. For model calibration, we implemented an iterative and robust parameter density estimation protocol to refine the parameter space and calibrate to temporal biological datasets (***Joslyn et al., 2021***). Partial rank correlation coefficient (PRCC) was used to guide in silico experiments by identifying parameters and timepoints that were most critical for ideal regeneration metrics.

Results

ABM outputs align with calibration and validation data

Following parameter density-based calibration, the unknown parameters were narrowed into a final calibration parameter set (***Supplementary file 1***). The simulations captured SSC and fibroblast cellular behaviors, as well as CSA outcomes, that aligned with experimental studies (***Figure 1***; ***Figure 2A–C***). The model data were consistent with the experimental trends, and the 95% confidence interval was within the standard deviation (SD) for all calibration data timepoints except for SSCs at day 3 (***Figure 2B***). Macrophage (total, M1, and M2), neutrophil, and capillary counts, which were not used for model calibration, were also found to be consistent with experimental trends and allowed us to independently validate model outputs (***Figure 2D–H***).

ABM perturbations are consistent with published experiments

Overall, the model reproduced findings from multiple studies, replicating how altered conditions lead to both improved and diminished muscle regeneration (***Figure 3***). Injections of vascular

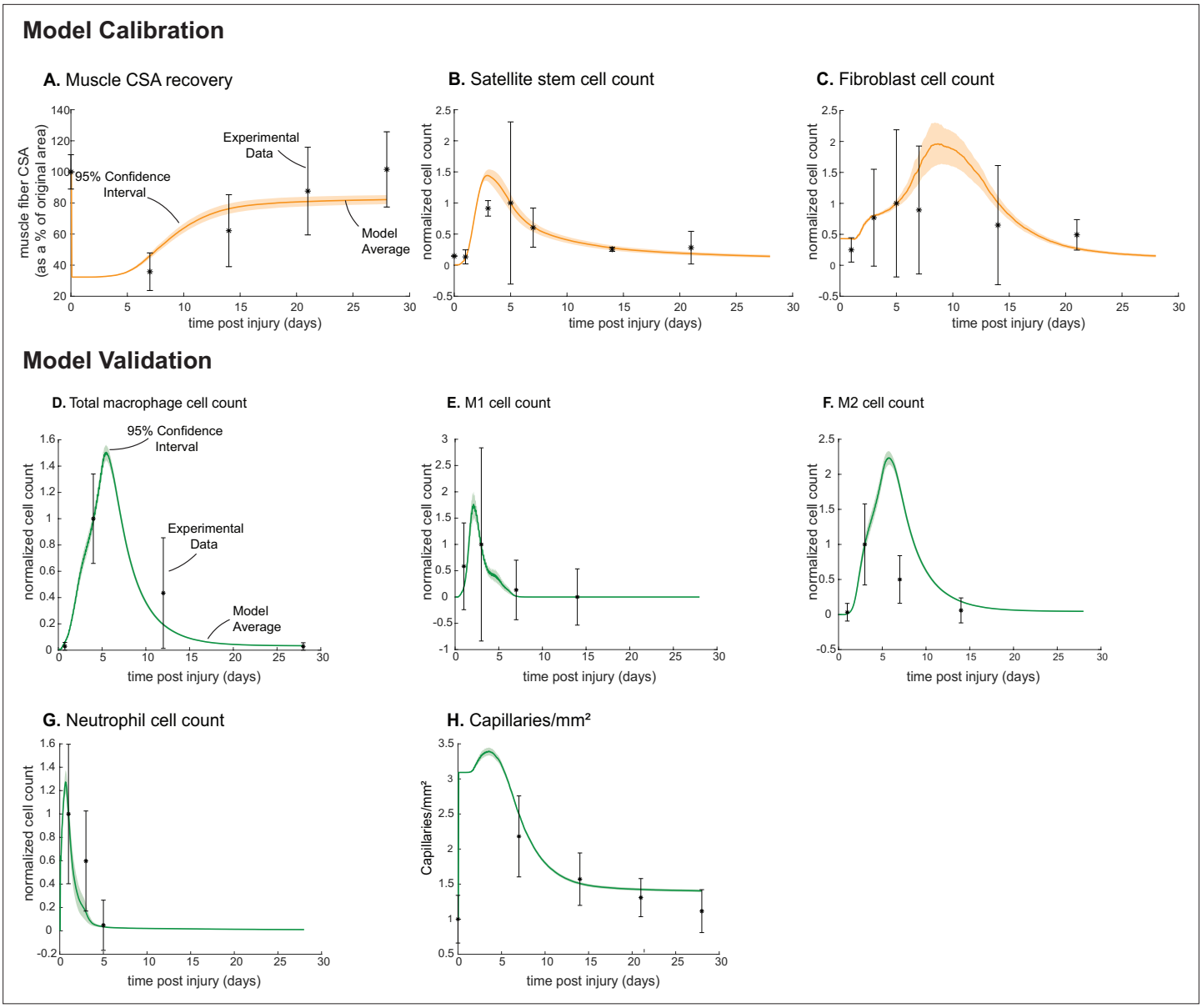

Figure 2. Agent-based model (ABM) calibration and validation. ABM parameters were calibrated so that model outputs for cross-sectional area (CSA) recovery, satellite stem cell (SSC), and fibroblast counts were consistent with experimental data (**A–C**). (***Murphy et al., 2011***; ***Ochoa et al., 2007***). Separate outputs from those used in calibration were compared to experimental data (***Hardy et al., 2016***; ***Ochoa et al., 2007***; ***Wang et al., 2018***; ***Nguyen et al., 2011***) to validate the ABM (**D–H**). Error bars represent experimental standard deviation, and model 95% confidence interval is indicated by the shaded region. Cell count data were normalized by number of cells on the day of the experimental peak to allow for comparison between experiments and simulations.

The online version of this article includes the following figure supplement(s) for figure 2:

Figure supplement 1. Overview of calibration methods.

endothelial growth factor A (VEGF-A) led to faster CSA recovery, more damaged tissue clearance, and a concentration-dependent dose response, consistent with prior studies (***Arsic et al., 2004***). Cell depletion simulations predicted decrease in all markers of regeneration, consistent with prior studies (***Arsic et al., 2004***; ***Teixeira et al., 2003***; ***Liu et al., 2017***). When simulating hindered angiogenesis conditions, the model aligned with experimental studies showing detriments in CSA recovery, increased neutrophil and macrophage cells, and elevated ECM collagen density, indicating progression of fibrosis within the microenvironment (***Hardy et al., 2019***). There were a few cases in which model predictions did not align with published studies. First, simulations of tumor necrosis

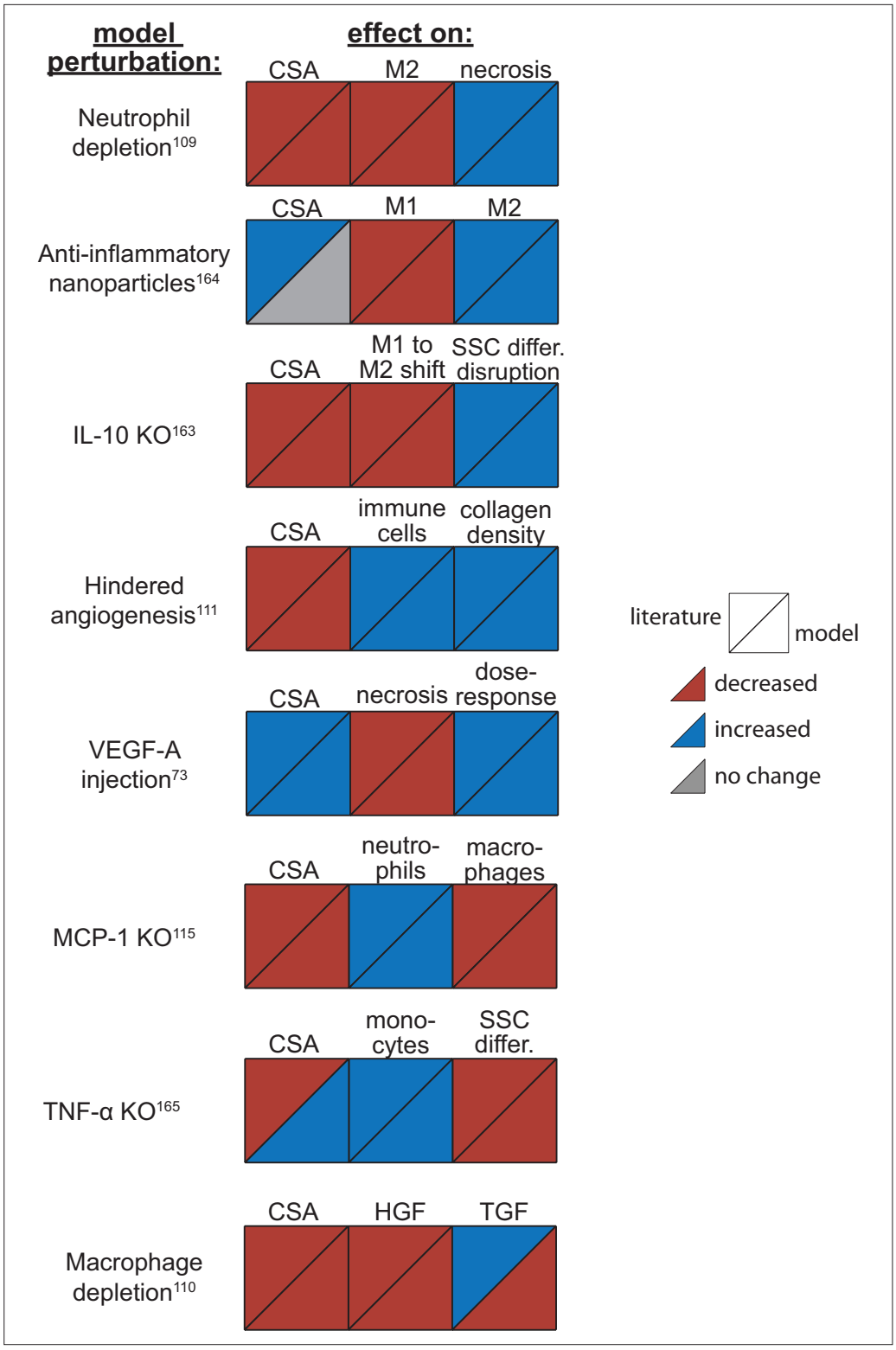

Figure 3. Agent-based model (ABM) perturbation outputs are compared to various literature experimental results. Each perturbation model output is compared to the available corresponding published result. The top triangles indicate the literature findings and the bottom triangles indicate the model outputs. Red triangles represent a decrease, blue represents an increase, and gray represents no significant change. Timepoints of comparison were based on which timepoints were available from published experimental data. Refer to ***Table 8*** for model input conditions and ***Supplementary file 7*** for information on experimental references.

factor alpha (TNF-α) knockout (KO) predicted increased CSA recovery, while experiments measured decreased recovery of CSA. This difference is likely due to the fact that the model did not include cross-regulation with interferons which are upregulated with TNF-α KO (***Cantaert et al., 2010***). Second, macrophage depletion simulations predicted decreased TGF-β concentrations throughout the simulation while experiments measured an initial decrease in concentration followed by increased concentrations at days 7 and 14. This difference may be due to the fact that macrophage depletion was experimentally induced with clodronate-containing liposomes which could have reduced consistency of depletion across the time course and other downstream impacts that were not represented by decreasing macrophages in the model perturbation (***Liu et al., 2017***).

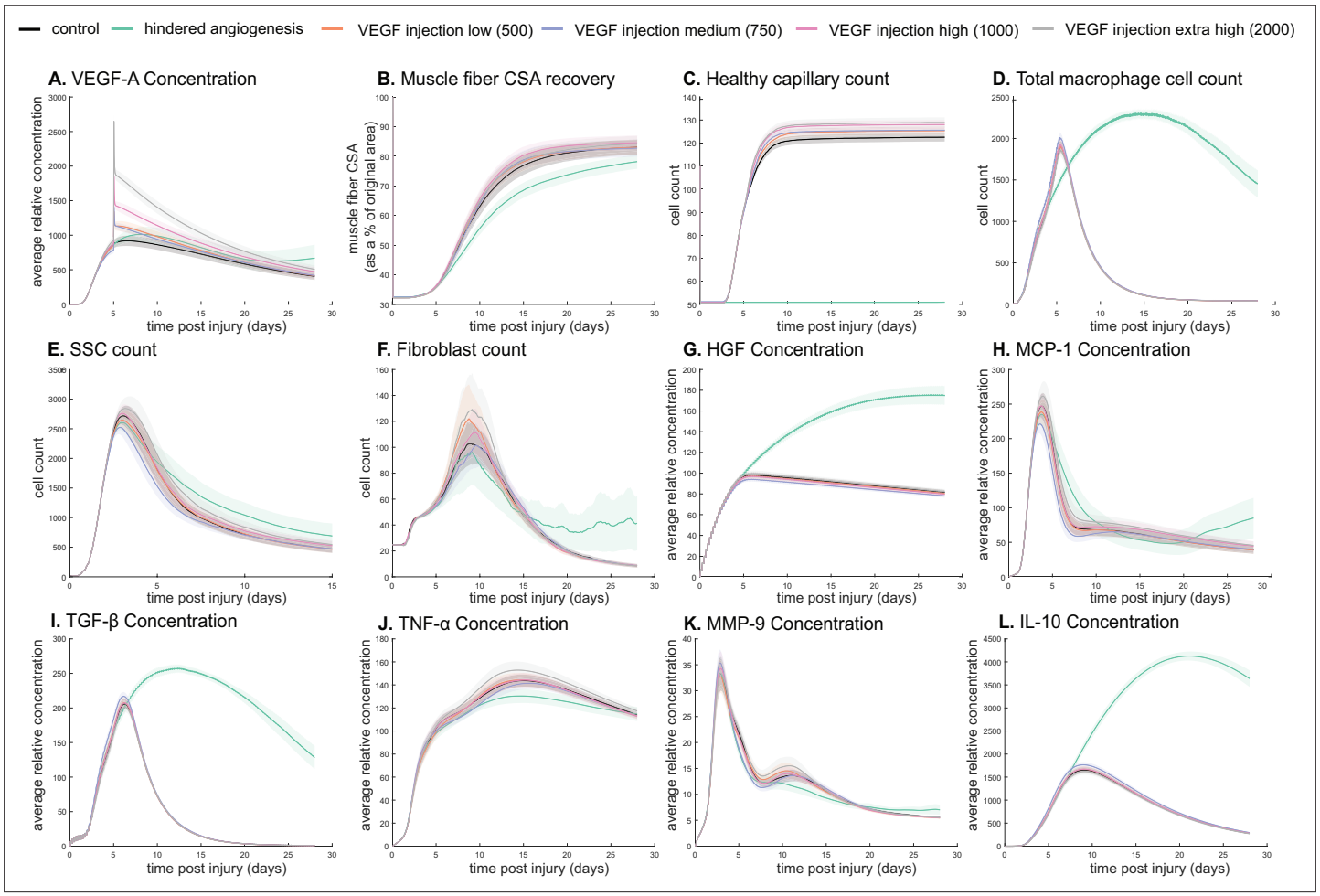

Figure 4. Dose-dependent response with vascular endothelial growth factor A (VEGF-A) injection compared to hindered angiogenesis. VEGF-A concentration response to varied levels of VEGF injection (**A**). Hindered angiogenesis resulted in slower and overall decreased cross-sectional area (CSA) recovery (**B**). Capillary count was dependent on VEGF-A injection level (**C**). Total macrophage count was similar between control and VEGF-A injection perturbations but macrophage count was higher in later timepoints in the hindered angiogenesis simulation (**D**). Satellite stem cell (SSC) peak varied with VEGF-A injection level and counts were prolonged in the hindered angiogenesis simulations (**E**). The fibroblast peak was lower for the hindered angiogenesis perturbation and highest with the extra high VEGF-A injection. In contrast to the other simulations, the fibroblast count was trending upward at later timepoints in the hindered angiogenesis perturbation (**F**). Hepatocyte growth factor (HGF) levels were consistent between control and VEGF-A injection perturbations but was significantly elevated in the hindered angiogenesis perturbation (**G**). Monocyte chemoattractant protein-1 (MCP-1), transforming growth factor beta (TGF-β), and interleukin 10 (IL-10) concentrations were elevated at later stages of regeneration with hindered angiogenesis (**H, I, L**). Tumor necrosis factor alpha (TNF-α) was elevated with the extra high VEGF-A injection and lower with hindered angiogenesis (**J**). Matrix metalloproteinase-9 (MMP-9) concentration was lower at the simulation midpoint but elevated at late regeneration stages (**K**).

Analysis of ABM perturbations leads to new insights regarding cytokine and cell dynamics

The model allowed for new insights into the dynamics of muscle regeneration by providing additional timepoints and metrics to evaluate the response to exogenous delivery of VEGF-A and hindered angiogenesis. VEGF-A levels remained elevated compared to control simulations following the injection at day 5 post injury (***Figure 4A***). CSA recovery had the highest increase at 28 days post injury with the high (10^3 relative concentration delivered) VEGF-A injection followed by the extra high (2×10^3 relative concentration delivered) injection (***Figure 4B***). The medium (750 relative concentration delivered) and low (500 relative concentration delivered) VEGF-A injections had higher CSA recovery 15 days post injury but were not significantly different from the control at day 28. All VEGF-A injections had a higher capillary count and were proportional to the level of VEGF-A injection (***Figure 4C***). The impact of VEGF-A injection on peak SSC and fibroblast counts was dependent on dosage amount, with the extra high VEGF-A injection resulting in the largest peaks (***Figure 4E and F***). Cytokine concentration

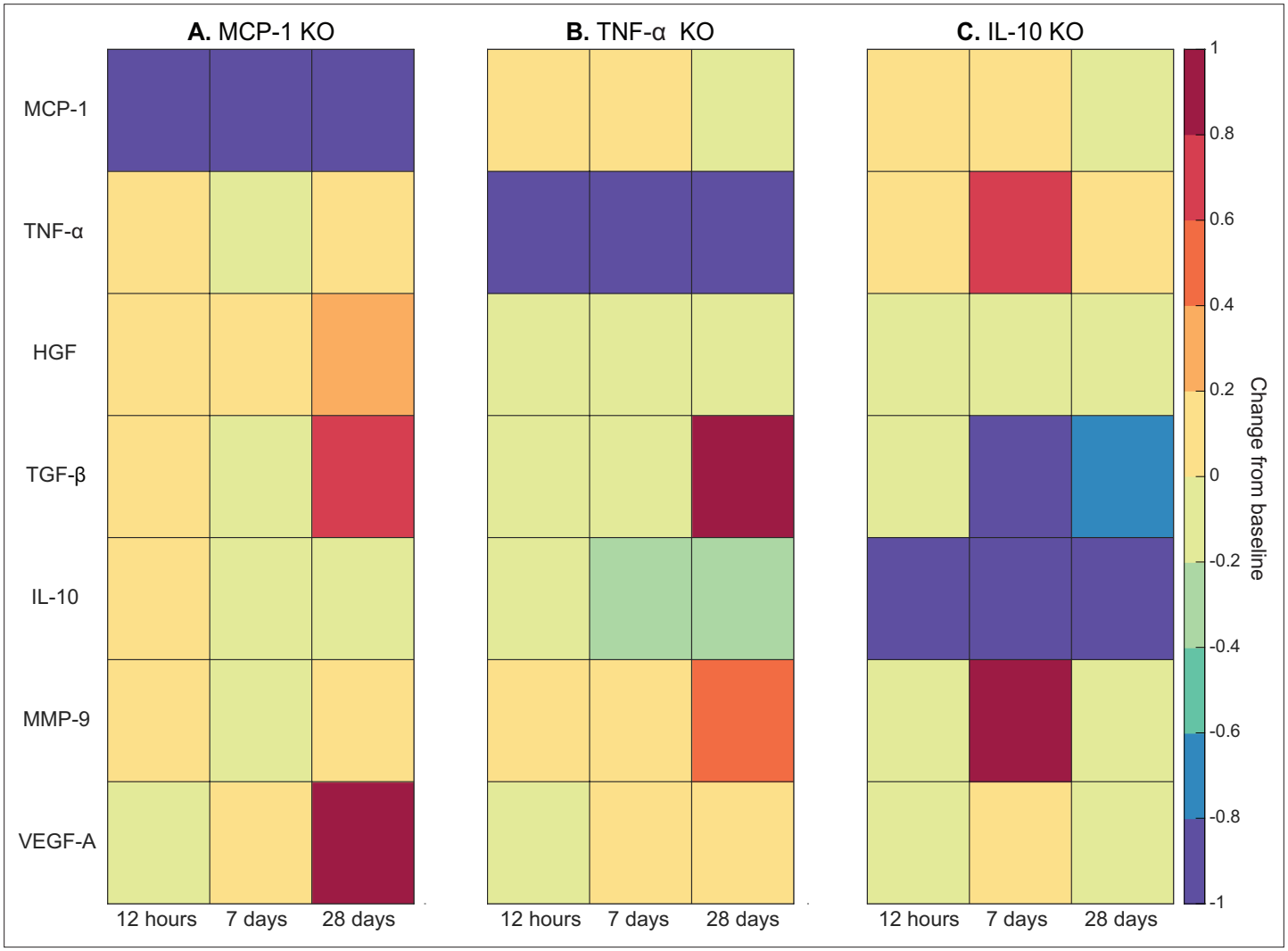

Figure 5. Heatmaps of changes in cytokine concentration at various timepoints throughout regeneration following individual cytokine knockout (KO) demonstrating cross-talk between cytokines. With monocyte chemoattractant protein-1 (MCP-1) KO there was an increase in all cytokines except vascular endothelial growth factor A (VEGF-A) at 12 hr post injury. Over the course of regeneration there was continued increasing elevation of hepatocyte growth factor (HGF), increases in VEGF-A, and transforming growth factor beta (TGF-β) decreased at day 7 followed by a strong increase by day 28 post injury (**A**). In the tumor necrosis factor-alpha (TNF-α) KO simulations, there was an early decrease in TGF-β that shifts to strong increases by day 28. Matrix metalloproteinase-9 (MMP-9) increased throughout the duration, HGF and interleukin 10 (IL-10) were decreased, VEGF-A lagged in the beginning but was increased during mid to late timepoints (**B**). Following IL-10 KO there were increases in TNF-α, decreases in HGF and TGF-β, and elevated MMP-9 at day 7 that decreased by day 28 (**C**).

trends were similar for all injections, but most peak levels were dosage dependent (***Figure 4G–L***). In contrast, hepatocyte growth factor (HGF) levels were elevated from days 5 to 28 with hindered angiogenesis, as were TGF-β and interleukin 10 (IL-10) (***Figure 4I and L***). Monocyte chemoattractant protein-1 (MCP-1) concentration had a lower overall peak level with elevated levels from days 21 to 28 (***Figure 4H***). Hindered angiogenesis had lower CSA recovery throughout the simulation and did not achieve unaltered regeneration levels (***Figure 4B***).

Cytokine KO perturbations revealed cross-talk and temporal interplay between cytokines (***Figure 5***). For example, with MCP-1 KO there was an overall increase in cytokine levels for all other cytokines within the microenvironment except for VEGF-A at 12 hr post injury (***Figure 5A***). By 7 days post injury TNF-α, TGF-β, IL-10, and matrix metalloproteinase-9 (MMP-9) had decreased from unaltered regeneration day 7 levels but VEGF-A and HGF were elevated. With TNF-α KO there was a decrease in TGF-β at early timepoints but a strong increase by day 28 (***Figure 5B***). Following IL-10 KO there was an increase in TNF-α that peaked at 7 days post injury (***Figure 5C***). HGF was slightly decreased throughout and TGF-β was strongly decreased by day 7. MMP-9 was decreased at 12 hr and 28 days post injury but heavily increased at day 7.

Cytokine dynamic analysis leads to new model perturbations that predict improved regeneration

Latin hypercube sampling (LHS)-PRCC of cytokine decay and diffusion parameters elucidated temporal relationships between cytokine parameters and key regeneration metrics, such as positive correlations between CSA and TGF-β and MMP-9 decay (Table 9). Of all cytokine parameters, the model outputs were most sensitive to HGF decay, with all outputs except M1 cell count being significantly impacted. PRCC plots showed that TGF-β and MMP decay were positively correlated and HGF decay was negatively correlated with CSA recovery, with higher significance at timepoints after 12 days (***Figure 6—figure supplement 1***). Correlation plots for various cytokine concentrations and regeneration metrics showed trends in cytokine-dependent cell behaviors such as the TNF-α concentration that led to heightened fibroblast cell counts as well as the corresponding TNF-α concentration threshold that results in diminished fibroblast response (***Figure 6—figure supplement 2***). These PRCC trends guided cytokine parameter perturbations to include lower HGF and VEGF-A decay, higher TGF-β, MMP-9, and MCP-1 decay, and higher MCP-1 diffusion because each of the cytokine modifications indicated some form of enhanced regeneration outcome metrics (***Supplementary file 2***). All these perturbations except MCP-1 decay show increased CSA, increased healthy capillaries, and increased SSCs (***Figure 6***). Finally, a combination of all changes except for MCP-1 decay was simulated. The combined cytokine alteration resulted in the highest CSA recovery (***Figure 6A***), as well as increased M1 macrophage counts (***Figure 6B***), decreased M2 macrophage counts (***Figure 6C***), increased fibroblasts (***Figure 6D***) and SSCs cell counts (***Figure 6E***). Capillaries regenerated faster in the combined perturbation than under unaltered conditions (***Figure 6F***, ***Figure 6—figure supplement 3***). It is likely that the combination of cytokines perturbed cell dynamics in a manner that promoted regeneration in both the early and later phases. During early regeneration, lower HGF decay, higher TGF decay, and MCP-1 diffusion contributed to increased SSCs while lowered VEGF decay increased angiogenesis. During late regeneration, lower HGF decay and higher MMP decay contributed to an increased anti-inflammatory state and SSC differentiation. The combined cytokine perturbation predicted a 13% improvement in CSA recovery compared to the unaltered regeneration amount at 28 days. The combined cytokine perturbation also had higher peaks in SSC and fibroblast counts than any of the singular cytokine perturbations, indicating the synergistic effects of altering the cytokine dynamics in combination.

Discussion

We developed a novel ABM that recapitulates muscle regeneration and, unique from prior work, includes spatial interactions between cytokines and the microvasculature based on relevant literature (***Westman et al., 2021***; ***Virgilio et al., 2018***; ***Martin et al., 2016***). The creation of the model provides a more controlled environment for studying muscle regeneration, reducing error and variation commonly encountered with in vivo experiments. Model predictions aligned with experimental data under various altered inputs. Through in silico experiments, we gained new insight into how the

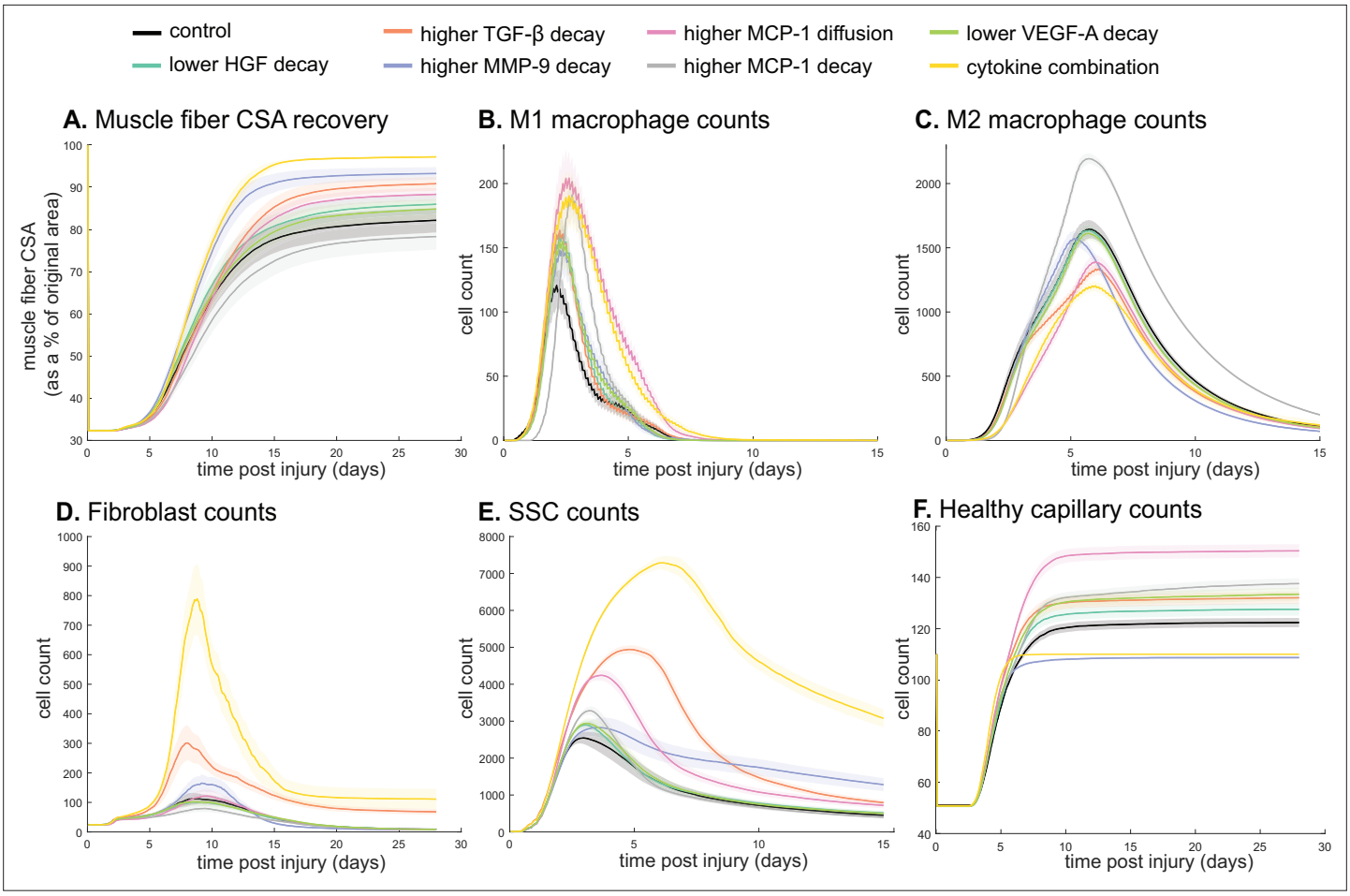

Figure 6. Combined alterations of various cytokine dynamics enhance muscle regeneration outcomes. All tested alterations except higher monocyte chemoattractant protein-1 (MCP-1) decay resulted in higher cross-sectional area (CSA) recovery compared to the control (**A**). M1 cell count was higher for all perturbations with the highest peaks with increased MCP-1 diffusion and the combined cytokine alteration perturbation (**B**). Higher MCP-1 decay resulted in the largest M2 peak and higher MCP-1 diffusion, higher transforming growth factor beta (TGF-β) decay, and the combined cytokine alteration had a lower M2 peak than the control (**C**). Fibroblasts had the largest increase in cell count with the higher TGF-β decay and the cytokine combination perturbations (**D**). All perturbations resulted in an increased satellite stem cell (SSC) count with the largest increase resulting from the combined cytokine alteration (**E**). All perturbations except the combined and higher matrix metalloproteinase-9 (MMP-9) decay resulted in increased capillaries as a result of additional capillary sprouts (**F**).

The online version of this article includes the following figure supplement(s) for figure 6:

Figure supplement 1. Partial rank correlation coefficient (PRCC) plots for various model outputs over time to illustrate how the significance of cytokine decay and diffusion parameters varies at different points throughout regeneration.

Figure supplement 2. Cytokine concentrations are correlated with cell counts and recovery metrics at various stages of regeneration.

Figure supplement 3. Non-perfused capillaries for each cytokine perturbation.

combination of key cytokine dynamic alterations could increase SSC cells and enhance CSA recovery. The ability for altered cytokine concentrations to change regeneration outcomes is consistent with studies that have found enhanced muscle recovery with delivery of platelet-rich plasma (PRP) which contain VEGF and TGF- β (***Kunze et al., 2019***). These model perturbations allow development of hypotheses and can provide the basis for future experiments and potential therapeutic interventions such as plasminogen activators to alter cytokines dynamics to enhance muscle recovery.

ABM provides biological insight on nonlinear effects of cytokine levels

The ABM offers valuable insights into the muscle regeneration dynamics under various altered conditions, elucidating the complex interplay of cytokines, angiogenesis, and cell behaviors. Systematic simulations reveal critical thresholds, nonlinear effects, and synergistic cytokine combinations

impacting regeneration. Perturbations varying VEGF-A injection doses showed increased CSA recovery up to a threshold (high VEGF-A injection simulation), beyond which further improvements in CSA recovery cease. Cytokine KO simulations revealed the complex nature of the relationship between cytokines; removal of one cytokine from the system has a cascading temporal impact. Relationships between cytokines and cellular outputs exhibit nonlinear effects, as seen with the limited impact of elevated HGF on CSA recovery beyond a threshold and the non-monotonic relationship between TNF-α and fibroblast counts (***Figure 6—figure supplement 2***). Further analysis revealed that specific combinations of cytokine perturbations could enhance regeneration beyond singular cytokine interventions. For example, a combined intervention of: (1) decreasing HGF and VEGF-A decay, (2) increasing TGF-β and MMP-9 decay, and (3) increasing MCP-1 diffusion enhanced muscle regeneration. Prior studies have shown that individually, increased HGF (***Choi et al., 2019***), VEGF-A (***Arsic et al., 2004***), and MCP- (***Liu et al., 2023***) stimulate muscle regeneration whereas reduced TGF-β (***Girardi et al., 2021***) and MMP-9 (***Zimowska et al., 2012***) stimulate muscle regeneration. The model suggests that combined alterations have a stronger regenerative effect than individual cytokine changes, enhancing muscle recovery through distinct mechanisms—increasing healthy capillaries, SSC counts, and reducing inflammatory cells.

Cytokine modifications intended to enhance muscle recovery can have clinical relevance and have been studied in various settings. For example, synthetic biomaterials coated with IL-4 have been implanted as a cytokine delivery vehicle and were successful in increasing M2 cells within the muscle (***Dziki et al., 2018***). Cytokine antagonist has been successful at promoting muscle regeneration, seen in prior work with anti-IL-6 (***Fujita et al., 2014***). Studies have also shown that activation of plasmin is able to induce the release of ECM-bound VEGF, increasing angiogenesis (***Ferrara, 2010***; ***Ismail et al., 2021***). Due to the complex network of cytokines, studies that deliver simple modulation of one or two cytokines typically have an insufficient response to generate appreciable improvements. This suggests that using a combination of biological and synthetic biomaterials to modulate multiple cytokines is necessary, which aligns with our findings (***Dziki et al., 2018***). Multiple cytokines have been modulated through the use of PRP which contains VEGF-A and an array of other cytokines, but PRP has had mixed success in a clinical setting (***Alsousou et al., 2013***). Our model has the capability to test and optimize various combinations of cytokines, along with exploring different temporal schedules for delivering specific treatments. For instance, it can predict whether modified combinations of cytokines prove beneficial at specific timepoints, aiding in the development of optimal treatment compositions aligned with the temporal dynamics of the regeneration cascade. These predictions provide novel concepts for future experiments and potential interventions. For example, the predictions from the model suggest that interventions that combine activation of plasmin for bound VEGF release (***Ferrara, 2010***; ***Ismail et al., 2021***) with delivery of synthetic biomaterials coated with HGF (***van de Kamp et al., 2013***), TGF-β antagonist (***Akhurst, 2002***), nuclear factor-kappa B inhibitory peptide to inhibit MMP-9 (***Li et al., 2009***), and recombinant MCP-1 hydrogels (***Lin et al., 2010***) to alter diffusion rate would result in improved regeneration outcomes.

Advancements from prior muscle regeneration models

Previous studies have employed computational models to investigate muscle regeneration across diverse contexts, such as Duchenne muscular dystrophy (DMD) and volumetric muscle loss (***Westman et al., 2021***; ***Virgilio et al., 2018***). Earlier muscle regeneration ABMs from our group have been used to test the effects of priming muscle with inflammatory cells prior to injury (***Martin et al., 2016***). While these models laid the foundation for simulating muscle adaptations, they were constrained by limited diffusion capabilities and an absence of critical features related to microvessel growth and remodeling throughout the regeneration process. Similarly, other ABMs from our group have examined altered microenvironments, but their omission of spatial cytokine diffusion hindered comprehensive representation of cell behaviors pivotal to regeneration (***Westman et al., 2021***; ***Virgilio et al., 2018***.) Recently, new ABMs have been published that focus on cerebral palsy and the impact of injury type on eccentric contraction-induced damage (***Khuu et al., 2021***; ***Khuu et al., 2023***).

The model presented here provides advancements over prior models in three areas: (1) explicit modeling of cytokine-specific diffusion and decay that depends on the ECM environment, (2) addition of microvasculature, and (3) incorporation of a robust and rigorous calibration and validation process. The addition of microvessel growth and remodeling dynamics empowers investigations into

how interventions impact angiogenesis during regeneration, thereby influencing muscle recovery outcomes. By considering the intricate relationship between microvessels and regeneration, our model opens avenues for evaluating the effects of interventions on the broader recovery process. Second, understanding how cytokines influence cell behaviors at different times during regeneration is crucial for determining optimal treatment targets and dosing. While cytokine dynamics can be altered experimentally, doing so is expensive and time-consuming (***Itoh, 2022***; ***Ferrara, 2010***) so exploring many combinations of alterations would be practically infeasible. Our model incorporates decay and diffusion dynamics of a subset of cytokines to allow testing of far more alterations in cytokines than would be reasonable to conduct experimentally. Lastly, we leveraged the CaliPro technique for parameter density estimation-based calibration and LHS-PRCC to gain biological insight by analyzing how altered microenvironmental parameters could benefit regeneration outcomes. This approach of implementing parameter identification to guide model perturbations demonstrates the capabilities of the model as a novel tool for generating new hypotheses and identifying mechanisms to target for enhanced regeneration outcomes.

Our model predictions are generally consistent with these prior models, with added biological complexity that has yielded several new important insights. For example, simulation of hindered angiogenesis predicted a decrease in SSCs leading to poor CSA recovery, similar to how lower SSC counts resulted in lower CSA recovery in perturbations in both healthy and DMD simulations (***Virgilio et al., 2018***). Our model provides additional understanding about the corresponding spatial cytokine changes that ultimately result in modulation of SSC dynamics within the microenvironment. The additional model advancements incorporated address prior muscle regeneration modeling gaps in understanding of how angiogenesis alters recovery outcomes as well as the response of complex spatial cell and cytokine dynamics.

Limitations and future work

There are some important limitations of this study that should be discussed. First, the model does not include all cell types and cytokines that are known to influence muscle regeneration and does not account for cytokine subtype or differences between endogenous and exogenous cytokines. These cells and cytokines likely have redundant functions, given the model effectively captures muscle regeneration using the included cells and cytokines. Second, the model does not currently represent hypertrophy during regeneration, which restricts CSA recovery from surpassing 100%; however, the cell dynamics it portrays remain consistent with those observed in studies that lead to hypertrophy following injury. Third, we assume a two-dimensional (2D) cross-section based on similar ABMs that have explored the relations of 2D to 3D simulations. These studies found that the diffusion accuracy is not greatly varied and that 2D is sufficient to predict the same mechanisms seen in 3D simulations (***Marino et al., 2018***; ***Sego et al., 2017***). To determine the robustness of the 2D initial cross-section, preliminary testing has shown that the initial spatial configuration can be altered and still achieve similar results (***Figure 1—figure supplement 1***), but further examination is needed to determine sensitivity to numerous configurations. Fourth, the calibration and validation dataset integrated multiple datasets from diverse sources. We acknowledge inherent limitations arising from variations in sample sizes and experimental techniques across sources. Fifth, it is also possible that the calibrated parameters are unable to capture behaviors that were not exhibited within the experimental datasets used in parameterization. While we tested ranges for each parameter and settled on a single parameter set that best fits the calibration data, there may be additional parameter sets that fit the calibration data but have varied levels of stochasticity and altered reproducibility of replicate simulations. Lastly, the current model was calibrated to male mice data despite known sex difference in skeletal muscle, regeneration mechanisms, and the timeline of recovery (***Haizlip et al., 2015***; ***Knewtson et al., 2022***; ***Liu et al., 2023***). Experimental measurements of female muscle regeneration are fairly limited because most muscle injury studies only use male mice or do not distinguish between sexes, making it difficult to incorporate sex differences into the model (***Enns and Tiidus, 2010***). Experiments that incorporate female mice and measure hormone levels are needed to accurately incorporate rules to distinguish between the sex-dependent dynamics of muscle regeneration.

This paper describes a significant advancement in modeling the complex process of muscle regeneration. Future efforts will extend the use of parameter density estimation to optimize the selection, doses, and timing of injections of exogenously delivered cytokines. Further refinement of analysis

methods could be pursued to disentangle specific underlying mechanisms of the dynamic feedbacks that drive the observed model outputs. Predictions from model simulations will also be used to inform future experiments by highlighting crucial timepoints to measure and predicted effect sizes for power analysis. Additionally, we aim to explore diverse muscle injury types and locations (i.e. injury relative to microvascular components) and their varying recovery responses, addressing challenges in comparing different acute injury techniques found in the literature. This study underscores the significance of cellular and cytokine spatial dynamics in muscle regeneration. Further inclusion of additional factors and hormones would provide a more holistic understanding of the system and how treatments may be altered based on microenvironmental conditions, providing a unique framework for the study of personalized muscle injury treatment.

Materials and methods

ABM development overview

ABMs represent the behaviors and interactions of autonomous agents, such as cells, which are governed by literature-derived rules (***Virgilio et al., 2018***; ***Martin et al., 2015***; ***Ferrari Gianlupi et al., 2022***). Agent-based modeling (ABM) provides an excellent platform for studying complex cellular dynamics because they reveal how the interactions between individual cellular behaviors lead to emergent behaviors in the whole system.

We implemented the ABM in CompuCell3D (version 4.3.1), a Python-based modeling software (***Swat et al., 2012***). The ABM's code is available for download (https://zenodo.org/records/10403014). To build the model, we extended upon about 40 rules developed in previous ABMs of

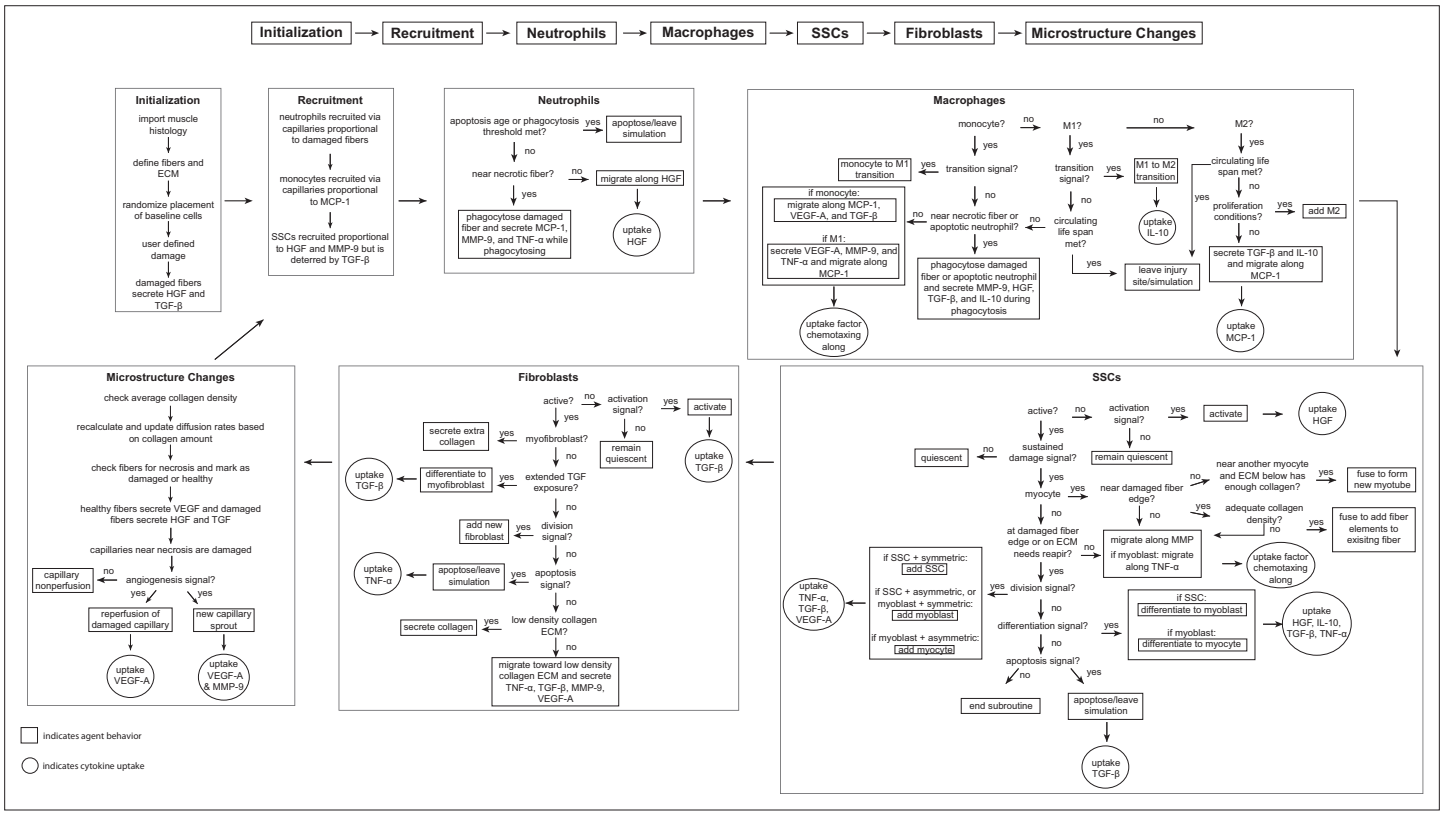

Figure 7. Flowchart of agent-based model (ABM) rules. The model starts with initialization of the geometry and the prescribed injury. This is followed by recruitment of cells based on relative cytokine amounts within the microenvironment. The inflammatory cells, SSCs, and fibroblasts follow their literature-defined rules and probability-based decision tree to govern their behaviors. The boxes represent the behavior that the agent completes during that timestep given the appropriate conditions and the circles represent the uptake that occurs as a result of the simulated binding with microenvironmental factors for certain cell behaviors. ABM, agent-based model; SSC, satellite stem cell; ECM, extracellular matrix; TGF-β, transforming growth factor beta; HGF, hepatocyte growth factor; TNF-α, tumor necrosis factor alpha; VEGF-A, vascular endothelial growth factor A; MMP-9, matrix metalloproteinase-9; MCP-1, monocyte chemoattractant protein-1; IL-10; interleukin 10.

muscle regeneration (***Westman et al., 2021***; ***Virgilio et al., 2018***; ***Martin et al., 2016***) in combination with a deep literature search referencing over 100 published studies to define approximately 100 total rules that dictate the behavior of fiber cells, SSC, fibroblasts, neutrophils, and macrophages, as well as their interactions with the microenvironment, including microvasculature remodeling and cytokine diffusion and secretion (***Figure 7***). For a rule to be incorporated into the model, there had to be an established understanding within the literature supporting the behavior (i.e. multiple studies reporting similar findings or supported by other reputable publications). When available, we used experimental data to define the parameters associated with the model rules. There were 52 parameters that could not be related to known physiological measurement; therefore, these parameters were calibrated using parameter density estimation which will be described below in *Model calibration*. Following calibration of model parameters, separate model outputs were validated by comparison with experimental data, and various model perturbations were conducted and compared to literature results. This process allowed us to have confidence in the predictive capabilities of the model so that we could simulate and predict the sensitivity of muscle regeneration to changes in cytokines.

Cellular-Potts modeling framework

Prior work to construct computational models to represent muscle recovery have used ordinary differential equation (***Stephenson and Kojouharov, 2018***) or agent-based modeling (ABM) software, such as Netlogo (***Martin et al., 2016***) or Repast (***Virgilio et al., 2021***). While these models have yielded great insights into skeletal muscle damage and recovery processes, they have limited capacity to represent the spatial diffusion of cytokines accurately and explicitly throughout the skeletal muscle. The Cellular-Potts model framework (***Swat et al., 2012***) (CPM, also known as the Glazier-Graner-Hogeweg model), proved an ideal choice because it allows for logic-based representation of cellular behavior and interactions characteristic of agent-based modeling (ABM) (see ***Supplementary file 3*** for CPM mathematical implementation, ***Supplementary file 4*** for CPM adhesion parameters).

ABM design

The ABM spatially represents a 2D male murine skeletal muscle fascicle cross-section of approximately 50 muscle fibers (***Figure 1***). The ABM depicts the microenvironment of the cross-section as well as the spatial migration of cells and diffusion of various cytokines (***Supplementary file 5***). The ABM simulates the emergent phenomenon of muscle tissue from an acute injury over the course of 28 days. The spatial agents in the model include muscle fibers, necrotic muscle tissues, ECM, capillaries, lymphatic vessels, quiescent and activated fibroblasts, myofibroblasts, quiescent and activated SSCs, myoblasts, myocytes, immature myotubes, neutrophils, monocytes, resident macrophages, pro-inflammatory macrophages (M1), and anti-inflammatory macrophages (M2). In addition, the ABM includes seven diffusing factors, such as HGF, MCP-1, MMP-9, TGF-β, TNF-α, VEGF-A, and IL-10. A review of the literature led us to determine that these factors and cytokine isoforms were most critical for representing the behaviors of each cell during the regeneration cascade (***Waldemer-Streyer et al., 2022***; ***Rucavado et al., 2002***).

The muscle cross-section geometry was created by importing a histology image stained with laminin α2 into a custom MATLAB script that masked the histology image to distinguish between the fibers and ECM. The mask was imported into an initialization CC3D script that defined the muscle fibers, ECM, and microvasculature to specific cell types and generated a PIF file that was imported into the ABM as the starting cross-section. The injury is simulated by stochastically selecting a region within the cross-section to replace the fiber elements with necrotic elements, where the percentage of CSA damage is an input parameter. When a threshold of fiber elements within a muscle fiber becomes damaged, the entire muscle fiber turns necrotic and requires clearance. If the damage is below the threshold, only the region of necrosis must be removed and the SSCs can fuse to the remaining fiber. During model initialization, the injury criteria can be altered to simulate various degrees of myotoxin injury by changing the percent of necrotic tissue following injury.

Each Monte Carlo step (mcs) represents a 15 min timestep, and the model simulations were run until 28 days post injury. The cell velocity is limited by how many times the Cellular-Potts algorithm is run, so we set 45 Cellular-Potts evaluations per mcs to ensure stability in migratory agent behavior. The number of Cellular-Potts evaluations per mcs and the lambda chemotaxis parameters were tuned in a simplified simulation of individual cells and their respective chemotactic gradients so we could

Table 1. Neutrophil agent rules.

Neutrophil agent behavior	Sources
Recruitment signal: necrosis	***Madaro and Bouché, 2014***
Neutrophils are brought to site of injury via capillaries	***Wang et al., 2020***
Phagocytose necrosis	***Butterfield et al., 2006***
Secretes MMP-9, MCP-1, TNF-α during phagocytosis	***Martin et al., 2016***; ***Madaro and Bouché, 2014***; ***Wang, 2018***; ***Soehnlein et al., 2008***
Undergoes apoptosis after phagocytosis or 12.5 hr	***Fox et al., 2010***
Migrates toward areas of high HGF	***Molnarfi et al., 2015***
Migration speed ~7.5 μm/min	***Zhao et al., 2020***; ***Heit et al., 2008***

obtain cell speeds that were consistent with speeds derived from literature sources (Table 7). At each mcs, the agent behaviors are governed by rules that were derived from experimental data found in the literature. The behaviors of each agent are based on environmental conditions, such as nearby cells and cytokine gradients, as well as probability-based rules. As an example, a capillary located near a damaged fiber has a probability of becoming non-perfused and then senses the amount of VEGF-A and MMP-9 at its location to decide if the levels are adequate to induce angiogenesis (Table 6). Model outputs include CSA recovery (sum of total healthy fiber elements normalized by the initial CSA), capillary and collagen density, cell counts, relative cytokine abundance, and spatial coordinates of cells and cytokines.

Table 2. Macrophage agent rules.

Macrophage agent behavior	Sources
Initial count: 1 resident macrophage per 5 myofibers	***Oishi and Manabe, 2018***
Recruitment signal: MCP-1	***Vogel et al., 2014***; ***Chazaud et al., 2003***
Monocytes are brought to the site of injury via microvessels	***Kratofil et al., 2017***
Resident macrophages secrete MMP-9, MCP-1, and TNF-α and chemotax along MCP-1 and HGF	***Elkington et al., 2009***; ***Chen and Nuñez, 2010***; ***Lacy and Stow, 2011***; ***Vogel et al., 2014***; ***Molnarfi et al., 2015***; ***Furrer and Handschin, 2017***
Monocytes chemotax along MCP-1, VEGF-A, and TGF-β	***Chazaud et al., 2003***; ***Owen and Mohamadzadeh, 2013***; ***Reibman et al., 1991***; ***Martin et al., 2017***
Monocyte migration speed ~4 μm/min	***van den Bos et al., 2020***
M1 macrophages secrete VEGF-A, MMP-9, and TNF-α and chemotax along MCP-1	***Corliss et al., 2016***; ***Newby, 2008***; ***Lu et al., 2018***; ***Cui et al., 2018***
Monocytes, resident, and M1 macrophages phagocytose apoptotic neutrophils and necrosis	***Greenlee-Wacker, 2016***; ***Watanabe et al., 2019***; ***Uribe-Querol and Rosales, 2020***
Monocytes and macrophages secrete MMP-9, HGF, TGF-β, and IL-10 during phagocytosis	***Martin et al., 2016***; ***Yoon et al., 2016***; ***D'Angelo et al., 2013***; ***Popov et al., 2010***; ***Arnold et al., 2007***; ***Chung et al., 2007***
Monocyte transitions into M1 occurs when TNF-α threshold is met or based on literature means and standard deviation properties	***Arnold et al., 2007***; ***Mosser and Edwards, 2008***
M1 transition into M2 is mediated by the amount of IL-10 and the amount the M1 has phagocytosed	***Martin et al., 2016***; ***Arnold et al., 2007***; ***Saini et al., 2016***; ***Das et al., 2015***
M2 macrophages secrete TGF-β and IL-10 and chemotax along MCP-1	***Martin et al., 2016***; ***Vogel et al., 2014***; ***Arabpour et al., 2021***; ***da Silva et al., 2015***
Macrophages can proliferate following the transition to the anti-inflammatory (M2) state	***Arnold et al., 2007***
Macrophage migration speed ~0.62 μm/min	***van den Bos et al., 2020***
Macrophages apoptose in a Poisson distribution	***Moncayo, 2007***

Table 3. SSC agent rules.

SSC agent behavior	Sources
Initial count: 1 SSC per 4 fibers	***Virgilio et al., 2018***; ***Reimann et al., 2000***
Recruitment signal: HGF + MMP-9 - TGF-β	***Virgilio et al., 2018***; ***Kawamura et al., 2004***; ***Wang et al., 2009***; ***Allen and Boxhorn, 1989***; ***González et al., 2017***
Activation signal: HGF	***Virgilio et al., 2018***; ***González et al., 2017***; ***Allen et al., 1995***; ***Miller et al., 2000***; ***Tatsumi et al., 1998***
Activated SSCs secrete MCP-1 and VEGF-A	***Chazaud et al., 2003***
Activated SSCs migrate toward areas of high MMP-9	***Wang et al., 2009***; ***Chen and Li, 2009***
Myoblasts migrate toward high TNF-α	***Torrente et al., 2003***
Division signal: TNF-α + VEGF-A - TGF-β	***Virgilio et al., 2018***; ***Allen and Boxhorn, 1989***; ***Bakkar et al., 2008***; ***Saclier et al., 2013***
Differentiation signal: 3*IL-10 - HGF - TNF-α - TGF-β	***Virgilio et al., 2018***; ***Saini et al., 2016***; ***Perandini et al., 2018***; ***Gal-Levi et al., 1998***; ***Ten Broek et al., 2010***
Activated SSCs differentiate into myoblasts, myoblasts into myocytes, and myocytes into myotubes/myofibers	***Cooper et al., 1999***; ***Flamini et al., 2018***; ***Bentzinger et al., 2012***
Differentiated myocytes fuse at damaged fiber edge or fuse together to form new, immature myotubes	***Yin et al., 2013***; ***Wang et al., 2014***; ***Nguyen et al., 2019***; ***Ruiz-Gómez et al., 2002***
50% cell divisions are symmetric, 50% asymmetric	***Virgilio et al., 2018***; ***Kuang et al., 2007***; ***Yennek et al., 2014***
Division probability decreases with each cell division; first division 85%; second 65%; third 20%	***Virgilio et al., 2018***; ***Siegel et al., 2011***
VEGF-A and macrophages nearby can block apoptosis	***Chazaud et al., 2003***; ***Arsic et al., 2004***; ***Sonnet et al., 2006***
TGF-β triggers apoptosis	***Cencetti et al., 2013***
Time to divide: 10 hr	***Virgilio et al., 2018***; ***Siegel et al., 2011***; ***Rocheteau et al., 2012***
Migration speed ~0.94 μm/min	***Otto et al., 2011***
Return activated SSCs to quiescence without sustained HGF	***González et al., 2017***

Overview of agent behaviors

Simulated behaviors (***Figure 1B***) of the neutrophils and macrophages include cytokine-dependent recruitment, chemotaxis, phagocytosis of damaged fibers (neutrophils, monocytes, and M1 macrophages), phagocytosis of apoptotic neutrophils (monocytes and M1 macrophages), secretion and uptake of cytokines, and apoptosis. The SSC and fibroblast agent behaviors also include cytokine-dependent recruitment, chemotaxis, secretion and uptake of cytokines, and apoptosis, in addition to quiescence, activation, division, and differentiation. The biological intricacy of some cell types, such as SSCs which have a more complex cell cycle and are regulated by dynamic interplay of intrinsic factors and an array of microenvironmental stimuli, led to the necessity for adding more rules that govern their behaviors (***Yin et al., 2013***).The neutrophils have 18 parameters for 7 agent rules (***Table 1***), macrophages have 31 parameters for 15 agent rules (***Table 2***), SSCs have 33 parameters dictating the 17 agent rules (***Table 3***), fibroblasts have 27 parameters for 11 agent rules (***Table 4***), fibers have 18 parameters for 4 agent rules (***Table 5***), and microvessels have 22 parameters for 6 agent rules (***Table 6***). At each mcs, cytokines are secreted by agents if certain conditions were met. For cell recruitment, the levels of recruiting cytokines for each agent are checked, and if the concentration is high enough to signal cell recruitment, a new agent is added to the field at the location of the highest concentration. The agents also undergo chemotaxis by sensing the surrounding cytokine gradients and move toward higher concentrations of cytokines, binding and removing that cytokine as they move along it to simulate physical binding of the cytokine to the receptor. Agents that are in a quiescent state require a certain threshold level of cytokines to become activated and cannot chemotax, secrete, divide, or differentiate until this threshold is reached. Our model assumes each unique cell type secretes the same concentration of cytokines per timestep for all relevant cytokines

Table 4. Fibroblast agent rules.

Fibroblast agent behavior	Sources
Initial count: 1 fibroblast per every 2 fibers	***Virgilio et al., 2018***; ***Murphy et al., 2011***
Activation signal: TGF-β	***Gibb et al., 2020***
Fibroblasts move to low collagen ECM	***Virgilio et al., 2018***; ***Dickinson et al., 1994***
Fibroblasts secrete TNF-α, TGF-β, MMP-9, VEGF-A. Collagen is secreted at low-density ECM	***Virgilio et al., 2018***; ***Zou et al., 2008***; ***Sanderson et al., 1986***; ***Yokoyama et al., 1999***; ***Skutek et al., 2001***; ***Lindner et al., 2012***; ***Newman et al., 2011***
Fibroblast division signaled by SSC division	***Virgilio et al., 2018***; ***Murphy et al., 2011***
Division probability decreases with each cell division; first division 100%; second 25%; third 6%	***Alberts et al., 2002***
Fibroblast differentiation into myofibroblasts with extended TGF-β exposure	***Virgilio et al., 2018***; ***Desmoulière et al., 1993***; ***Wipff et al., 2007***
Myofibroblasts secrete double the amount of collagen and secretion is not dependent on collagen density	***Virgilio et al., 2018***; ***Petrov et al., 2002***
Fibroblasts apoptose with sustained exposure to TNF-α	***Virgilio et al., 2018***; ***Lemos et al., 2015***
Fibroblast migration speed ~0.73 μm/min	***Cornwell et al., 2004***
Sufficient TGF-β can block fibroblast apoptosis	***Virgilio et al., 2018***; ***Lemos et al., 2015***

to drive model agent decisions. Each computational timestep represents 15 min of real-world time. We assume that this is of sufficient resolution to accurately reproduce immune cell agent behaviors during regeneration.

Neutrophil agents

Neutrophils are recruited through capillaries to sites of necrotic tissue (***Table 1***). Neutrophils move to areas of necrotic tissue with high concentrations of HGF by chemotaxing along the HGF gradient to reach areas of necrosis (***Madaro and Bouché, 2014***; ***Wang et al., 2020***). Neutrophils phagocytose necrotic tissue and facilitate remodeling into ECM with low collagen density. During phagocytosis, neutrophils secrete MMP-9, MCP-1, and TNF-α (***Butterfield et al., 2006***; ***Madaro and Bouché, 2014***; ***Wang, 2018***; ***Soehnlein et al., 2008***). Individual neutrophil agents apoptose after phagocytosing two necrotic cells (based on calibration) or 12.5 hr after their recruitment (***Fox et al., 2010***).

Macrophage agents

Resident macrophages are distributed randomly throughout the tissue at a ratio of 1 macrophage per 5 myofibers at model initialization and secrete MCP-1 (***Oishi and Manabe, 2018***; ***Table 2***). Resident macrophages chemotax along MCP-1 and HGF chemical gradients and secrete MMP-9, TNF-α, and MCP-1 during simulation (***Elkington et al., 2009***; ***Chen and Nuñez, 2010***; ***Lacy and Stow, 2011***; ***Vogel et al., 2014***; ***Molnarfi et al., 2015***; ***Furrer and Handschin, 2017***). After tissue injury, monocytes are recruited through healthy capillary microvasculature and chemotax along MCP-1, VEGF-A, TGF-β (***Kratofil et al., 2017***; ***Chazaud et al., 2003***; ***Owen and Mohamadzadeh, 2013***; ***Reibman et al., 1991***). Monocytes infiltrate into the tissue if the MCP-1 concentration is above a specified threshold at a capillary site. Resident macrophages, monocytes, and the M1 macrophages differentiated from

Table 5. Fiber agent rules.

Fiber agent behavior	Sources
Damaged muscle fibers secrete HGF and TGF-β	***Miller et al., 2000***; ***Kim and Lee, 2017***
Healthy fibers secrete VEGF-A	***Huey, 2018***
Fibers that are fully necrotic are fusion incompetent, but damaged fibers are fusion competent	***Snijders et al., 2015***
Immature myotubes gain functional capacity as they fully mature over time	***Nguyen et al., 2019***; ***Abmayr and Pavlath, 2012***; ***Isesele and Mazurak, 2021***

Table 6. Microvasculature rules.

Microvessel agent behavior	Sources
Initial count: ~4 capillaries per fiber, 1 lymphatic vessel per fascicle	***Wickler, 1981***; ***Gehlert et al., 2010***
Capillaries near necrosis will become damaged and unable to perfuse	***Jacobsen et al., 2021***
With sufficient VEGF-A damaged capillaries will undergo angiogenesis	***Frey et al., 2012***
MMP-9 is elevated during capillary growth	***Haas et al., 2000***; ***Qutub et al., 2009***
Increasing capillary-to-myofiber ratio during muscle regeneration from new sprouting capillaries at areas with enough MMP-9 and VEGF-A	***Jacobsen et al., 2021***; ***Hardy et al., 2016***; ***Haas et al., 2000***
Cells and cytokines near lymphatic vessel will be drained via the vessel and removed from microenvironment	***Hampton and Chtanova, 2019***

monocytes may phagocytose areas of necrotic tissue and apoptotic neutrophil agents (***Greenlee-Wacker, 2016***; ***Watanabe et al., 2019***; ***Uribe-Querol and Rosales, 2020***). During phagocytosis, these agents secrete MMP-9, HGF, TGF-β, and IL-10 (***Yoon et al., 2016***; ***D'Angelo et al., 2013***; ***Popov et al., 2010***; ***Arnold et al., 2007***; ***Chung et al., 2007***).

Monocytes transition to M1 polarized macrophages when the monocyte agent experiences a large enough TNF-α concentration or if enough time has passed that a predefined transition time threshold is met. Each monocyte agent at creation has a defined transition time sampled from a Gaussian distribution with mean and SD set to reproduce literature-defined populations of M1 macrophages over time (***Arnold et al., 2007***; ***Mosser and Edwards, 2008***).

M1 macrophages may transition to M2 macrophages if the M1 macrophage agent experiences an IL-10 concentration that exceeds a threshold value or if the M1 macrophage has phagocytosed enough to meet a calibrated threshold value (as discussed in *Model calibration*) (***Arnold et al., 2007***; ***Saini et al., 2016***; ***Das et al., 2015***). Following the transition to the anti-inflammatory phenotype, the M2 macrophages can proliferate, secrete TGF-β and IL-10, and chemotax along an MCP-1 gradient (***Vogel et al., 2014***; ***Arnold et al., 2007***; ***Arabpour et al., 2021***).

SSC agents

The model is initialized with 1 quiescent SSC per every 4 fibers and upon injury (***Reimann et al., 2000***). Additional SSCs are recruited based on the amount of HGF, MMP-9, and TGF-β (***Kawamura et al., 2004***; ***Wang et al., 2009***; ***Allen and Boxhorn, 1989***; ***González et al., 2017***; ***Table 3***). For SSC activation there has to be enough HGF at the location of the quiescent SSC to induce activation (***González et al., 2017***; ***Allen et al., 1995***; ***Miller et al., 2000***; ***Tatsumi et al., 1998***). The SSCs also chemotax up the MMP-9 gradient, removing some of the MMP-9 as they move along it. Activated SSCs can also undergo symmetric or asymmetric division and differentiation given that the required cytokine signaling is met locally. Activated SSCs differentiated into myoblasts and myoblasts differentiate into myocytes (***Cooper et al., 1999***; ***Flamini et al., 2018***; ***Bentzinger et al., 2012***). Myocytes can fuse to other myocytes to form new myotubes or fuse to fibers as long as the fiber is not fusion incompetent (i.e. fully necrotic) (***Yin et al., 2013***; ***Wang et al., 2014***; ***Nguyen et al., 2019***; ***Ruiz-Gómez et al., 2002***). Maturation of myotubes is required for fusion of additional myocytes to the new fiber (***Nguyen et al., 2019***; ***Abmayr and Pavlath, 2012***; ***Isesele and Mazurak, 2021***). If the damage signal is not sustained, activated SSCs return to quiescence. If there is enough TGF-β to induce apoptosis and not enough VEGF-A or macrophages nearby to block it, the SSC undergoes cell death and leaves the simulation (***Chazaud et al., 2003***; ***Arsic et al., 2004***; ***Sonnet et al., 2006***; ***Cencetti et al., 2013***).

Fibroblast agents

For model initialization, fibroblasts are randomly placed within the ECM at a population size that is proportional to the number of fibers (***Murphy et al., 2011***; ***Table 4***). Fibroblasts are activated based on the concentration of TGF-β around the fibroblast (***Beanes et al., 2003***; ***Chellini et al., 2019***). Fibroblasts include an additional expression in their effective energy function that directs their migration toward areas of low-density collagen ECM (***Dickinson et al., 1994***). Specifically, fibroblasts can form spring-like links to drag them toward areas of low-density ECM which are implemented with the

relation $\lambda_{ij}\left(l_{ij}-L_{ij}\right)^2$, where λ_{ij} denotes a Hookean spring constant of a link between cells *i* and *j*, *l* represents the current distance between the centers of mass between the two cells (in our case, fibroblast and low collagen ECM), and *L* is the target length of the spring-like link. In addition to the cytokines secreted by fibroblasts (***Table 4***), collagen is secreted at low-density collagen ECM (***Zou et al., 2008***; ***Sanderson et al., 1986***; ***Yokoyama et al., 1999***; ***Skutek et al., 2001***; ***Lindner et al., 2012***; ***Newman et al., 2011***). Fibroblasts divide when they are near dividing SSCs and can differentiate into myofibroblasts with extended exposure to TGF-β (***Murphy et al., 2011***; ***Desmoulière et al., 1993***; ***Wipff et al., 2007***). The myofibroblasts can secrete more collagen regardless of the ECM density (***Petrov et al., 2002***). Fibroblasts can undergo apoptosis if there are adequate levels of TNF-α at the site of the cell but it can be blocked if there is sufficient TGF-β (***Lemos et al., 2015***).

ECM agents

ECM elements surround the fiber elements and are assigned a collagen density parameter which varies based on the amount of necrotic tissue removed and the extent of fibroblast/myofibroblast collagen secretion. When necrotic elements are removed, the phagocytosing inflammatory cells secrete MMP-9s which degrade some of the collagen within that section of the ECM, thereby causing that element to have a lower collagen density (***Madaro and Bouché, 2014***). The collagen density of the ECM alters the diffusivity of the secreted factors, and fiber placement is dependent on the collagen density (discussed below). The fibroblasts help rebuild the ECM by secreting collagen on low collagen density ECM elements (***Zou et al., 2008***). Myofibroblasts can secrete collagen on any ECM element and if prolonged results in high-density collagen elements, representing a fibrotic state.

Fiber and necrotic agents

Upon model initialization, a portion of the muscle fiber agents are converted to necrotic fibers based on the user prescribed injury. Fibers that reach a damaged threshold became fully necrotic whereas those surrounding the area of necrosis were damaged but not fully apoptotic cells. Healthy fiber elements secrete VEGF-A, and necrotic elements secrete HGF and TGF-β (***Miller et al., 2000***; ***Kim and Lee, 2017***; ***Huey, 2018***; ***Table 5***). Phagocytosing agents chemotax along those gradients to clear the necrosis, but before a new fiber can be deposited, the collagen has to be restored so that there is a scaffold to hold the fiber in place (***Oishi and Manabe, 2018***). Fully necrotic fibers are fusion incompetent and require myocyte-to-myocyte fusion to form a new myofiber and require maturation before additional myocyte fusion (***Nguyen et al., 2019***; ***Abmayr and Pavlath, 2012***; ***Isesele and Mazurak, 2021***). Damaged fibers are regenerated by myocytes fusion to the healthy fiber edge (***Snijders et al., 2015***).

Capillary and lymphatic agents

The muscle fascicle environment includes approximately 4 capillaries per fiber and 1 lymphatic vessel (***Wickler, 1981***; ***Gehlert et al., 2010***; ***Table 6***). The model defines perfused capillaries as capillary agents that can transport neutrophils and monocytes into the system proportional to the concentration of recruiting cytokines (***Wang et al., 2020***; ***Kratofil et al., 2017***). The neutrophils and monocytes are added to the simulation at the lattice sites above capillaries (within the cell layer; ***Figure 1B***) and chemotax along their respective gradients. The recruitment of the neutrophils and monocytes are distributed among the healthy capillaries with a higher affinity for capillaries at locations with higher concentrations of HGF and MCP-1, respectively. Under physiologically reasonable chemotactic gradient conditions, the recruited immune cells dispersed efficiently, with no aggregation. Capillaries that are neighboring areas of necrosis become non-perfused and therefore are unable to transport cells into the microenvironment until regenerated (***Jacobsen et al., 2021***). Angiogenesis can occur as long as there is enough VEGF-A present at the non-perfused capillary (***Frey et al., 2012***). Similar to published studies, there is an increase in the capillary-to-myofiber ratio during muscle regeneration, which is due to the formation of new capillary sprouts modulated in part by local MMP-9 and VEGF-A levels (***Jacobsen et al., 2021***; ***Hardy et al., 2016***; ***Haas et al., 2000***).

The lymphatic vessel uptakes cytokines at lattice locations corresponding to the lymphatic vessel and will remove cells located in lattice sites neighboring those corresponding to the lymphatic vessel (***Hampton and Chtanova, 2019***). In addition, we have included a rule in our ABM to encourage cells to migrate toward the lymphatic vessel utilizing CompuCell3D External Potential Plugin

Table 7. Model parameters of spatial mechanisms.

Parameter	Value	Source/justification
Volume parameters		
Target volume neutrophil	12	Chosen for an average cell diameter of 12 μm (***Tigner et al., 2021***)
Target volume SSC	10	Chosen for an average cell diameter of 10 μm (***Garcia et al., 2018***)
Target volume macrophage	21	Chosen for an average cell diameter of 21 μm (***Krombach et al., 1997***)
Target volume monocyte	8.5	Chosen for an average cell diameter of 8.5 μm (***Downey et al., 1990***)
Target volume fibroblast	15	Chosen for an average cell diameter of 15 μm (***Freitas, 1999***)
Volume multiplier λ_{volume}	50	Volume constraint to maintain target (***Swat et al., 2012***)
Diffusion coefficients		
HGF	66.38 $\mu m^2/s$	
MMP-9	63.40 $\mu m^2/s$	
MCP-1	189.27 $\mu m^2/s$	
VEGF-A	112.10 $\mu m^2/s$	
TGF-β	90.33 $\mu m^2/s$	
TNF-α	138.95 $\mu m^2/s$	Estimated diffusivity within the ECM accounting for baseline GAGs and collagen (***Filion and Popel, 2005***)
IL-10	135.17 $\mu m^2/s$	
Chemotaxis parameters λ_c		
Neutrophils	750	Chosen for a cell velocity between 1 and 20 μm/min (***Zhao et al., 2020***)
Macrophage	9.3	Chosen for a cell velocity around 0.62 μm/min (***van den Bos et al., 2020***)
Monocyte	75	Chosen for a cell velocity around 4 μm/min (***van den Bos et al., 2020***)
SSC	11.3	Chosen for a cell velocity around 0.94 μm/min (***Otto et al., 2011***)
Fibroblast	23	Chosen for a cell velocity around 0.73 μm/min (***Westman et al., 2021***)

(***ExternalPotential Plugin, 2024***). The influence of this rule is inversely proportional to the distance of the cells to the lymphatic vessel.

Binding, diffusivity, and collagen density

For many of the agent behaviors described above, there are associated binding events that play key roles in regulation of the cytokine fields. Any cytokine-dependent behavior is coupled with removal of a portion of that cytokine once the behavior is initiated. For example, upon SSC activation the amount of HGF required to activate is taken up by the SSC and removed from the cytokine field to simulate the ligand binding and endocytosis resulting from SSC activation. Similar binding events were modeled for SSC and fibroblast division and differentiation, macrophage transitions, cell apoptosis, and chemotaxis along a cytokine gradient.

Due to limited data availability quantifying the diffusion constants of the modeled cytokines in the context of the tissue microenvironment (which includes diffusion-altering elements including collagen and glycosaminoglycans [GAGs]), we applied a diffusivity estimation technique (***Filion and Popel, 2005***). To do so, previously developed methods (***Equation 1***) were applied to account for the

combined effects of collagen and GAGs (***Table 7***; ***Filion and Popel, 2005***). The expression includes the radius of the cytokine (r_s), the radius of the fiber (r_f), the volume fraction (ϕ), D and D_∞ are the diffusivities of the cytokines in the polymer solution and in free solution, respectively. This estimation technique allowed for consistent conditions for cytokine diffusion calculations and fluctuations based on changes in collagen density within the model.

$$D = D_\infty \left(-\phi^{\frac{1}{2}} \frac{r_s}{r_f} \right)_{collagen} \times exp \left(-\phi^{\frac{1}{2}} \frac{r_s}{r_f} \right)_{GAG} \quad (1)$$

Throughout the model simulation, the diffusivity is recalculated with the updated collagen volume fraction, as the collagen density changes throughout the microenvironment. This allows the changes in collagen density within the ECM to be reflected in the diffusion rate of each of the cytokines in the model.

Model calibration

Known parameters were fixed to literature values, and uncertain parameters were calibrated by comparing simulation outcomes to published experimental data. Calibration data included published findings from injury models that have synchronous regeneration after tissue necrosis (i.e. cardiotoxin, notexin, and barium chloride) (***Hardy et al., 2016***). The metrics that were used to calibrate the model included time-varying CSA (***Ochoa et al., 2007***), SSC counts (***Murphy et al., 2011***), and fibroblast counts (***Murphy et al., 2011***). These metrics were used for calibration because of their key roles in the regeneration of muscle and the complex interplay between these outputs. Cell count data were normalized by the number of cells on the day of the experimental peak to allow for comparison between experiments and simulations. For CSA, the experimental and model outcomes were normalized using fold-change from pre-injury to compare model-simulated with experimental CSA, as percent change from baseline is commonly used experimentally (***Pratt et al., 2015***; ***You et al., 2023***). Model cell counts were normalized by the number of cells at the peak timepoint in the experimental data. SSC and fibroblast counts were normalized to day 5. Neutrophil counts were normalized to day 1. Total macrophage, M1, and M2 counts were normalized to day 3. The capillaries were normalized to fiber area, as done in the experimental data.

Initial ranges for the 52 unknown parameters were determined by literature review or by running the model to test possible upper and lower thresholds for parameters (***Supplementary file 1***). To narrow the parameter ranges beyond those initial ranges, we used a recently published calibration protocol, CaliPro, which utilizes parameter density estimation to refine parameter space and calibrate to temporal biological datasets (***Joslyn et al., 2021***). CaliPro was selected as the calibration method because it is model-agnostic which allows it to handle the complexities of stochastic models such as ABMs, selects viable parameter ranges in the setting of a very high-dimensional parameter space, and circumvents the need for a cost function, a challenge when there are many objectives, as in our case. Briefly, Latin hypercube sampling (LHS) was used to generate 600 samples which were run in triplicate. These runs were then evaluated against a set of pass criteria, and the density functions of the passing runs and failing runs were calculated (***Supplementary file 6***). Parameter ranges were narrowed by alternative density subtraction, where the new ranges were determined by the smallest and largest parameter values where the density of passing is higher than the density of failing. The sensitivity of the model outputs to the parameters was examined using LHS in combination with PRCC (***Marino et al., 2008***). LHS/PRCC methods have been used for various differential equation models and ABMs (***Segovia-Juarez et al., 2004***). PRCC was computed using MATLAB to determine the correlation between ABM parameters (i.e. cytokine threshold for activation) and the ABM output (i.e. fibroblast cell count). Correlations with a p-value less than 0.05 were assumed to be statistically significant. This helped refine initial parameter bounds as well as make model adjustments based on the parameter dynamics elucidated from PRCC. This process of sampling parameter ranges, evaluating the model, and narrowing parameter ranges was repeated in an iterative fashion while updating pass criteria until a parameter set was identified that consistently met the strictest criteria (***Figure 2—figure supplement 1***). The final passing criteria were set to be within 1 SD of the experimental data for CSA recovery and 2.5 SD for SSC and fibroblast count. These criteria were selected so that the model followed experimental trends and accounted for both model stochasticity and experimental variability

Table 8. Model perturbation input conditions and corresponding published experimental results.

Perturbation	Specific model conditions	Published outcomes
IL-10 knockout	Adjust diffusion and decay parameters so IL-10 is removed from the system	Attenuates shift to M2, disrupted SSC differentiation, slowed regeneration (***Deng et al., 2012***)
Neutrophil depletion	Lower neutrophil recruitment proportion	Abundant necrotic tissue 7 days post injury (***Teixeira et al., 2003***)
Macrophage depletion	Lower macrophage recruitment proportion	Decreased HGF, increased TGF-β and TNF-α, impaired regeneration (***Liu et al., 2017***)
MCP-1 knockout	Adjust diffusion and decay parameters so MCP-1 is removed from the system	Increased necrosis at day 7, lower CSA at day 21, impaired phagocytosis (***Lu et al., 2011***)
Directed M2 polarization (anti-inflammatory nanoparticles)	Require less phagocytosis and IL-10 for transition	Improved muscle histology and inflammatory resolution (***Raimondo and Mooney, 2018***)
TNF-α knockout	Adjust diffusion and decay parameters so TNF-α is removed from the system	Impaired recovery at days 5 and 12, increased inflammation (***Chen et al., 2005***)
Hindered angiogenesis	Increase VEGF-A and MMP-9 threshold required for angiogenesis	Delayed regeneration with toxin injury, and persistent immune cell infiltration with freeze injury (***Hardy et al., 2019***)
VEGF-A injection	Add VEGF-A at specified concentration (100 for low and 1000 relative concentration for high), radius (300 pixels), and timepoint (5 days post injury)	Lower injury area at day 20 post injury with injection 5 days after damage (***Arsic et al., 2004***)

in datasets that had narrower SDs for certain timepoints. Early iterations had a wide parameter range to avoid missing portions of the realistic parameter space. At first, narrowing the parameter space increased passing simulations, but upon reaching the ideal parameter space, further narrowing eliminated viable parameters, resulting in fewer passing runs. Following eight iterations of narrowing the parameter space with CaliPro, we reached a set of parameters that had fewer passing runs than the previous iteration. We then returned to the runs from the prior iteration and set the bounds such that all three runs from the parameter set fell within the final passing criteria. The final parameter set was run 100 times to verify that the variation from the stochastic nature of the rules did not cause output that was inconsistent with experimental trends.

Model validation

We compared model outputs M1, M2, and total macrophage counts (***Hardy et al., 2016***; ***Wang et al., 2018***), neutrophil counts (***Nguyen et al., 2011***), and capillary counts (***Ochoa et al., 2007***) that were kept separate from the calibration criteria with published experimental data to verify that these outputs followed trends from the experimental data without requiring extra model tuning. In addition, we also altered various model input conditions (cell input conditions, cytokine dynamics, and microvessel dynamics) to simulate an array of model perturbations (***Table 8***) which allowed comparison of a set of model outputs with separate published experiments (***Supplementary file 7***). For example, we simulated an IL-10 KO condition by eliminating IL-10 secretion and adjusting the diffusion and decay parameters so that the concentration of IL-10 throughout the simulation was reduced, decreasing the behaviors driven by the cytokine as a result of the KO condition. One hundred replicates of each model perturbation were performed, and perturbation outputs were compared with control simulation outputs via a two-sample t-test with a significance level of 0.05. We were then able to compare how the model outputs aligned with published experimental findings to determine if the model could capture the altered regeneration dynamics.

Sensitivity analysis

A sensitivity analysis was performed using LHS-PRCC to examine the impact of cytokine-related parameters on model outputs of interest. Diffusion coefficients and decay rates for the seven cytokines (HGF, TGF-β, MMP-9, TNF-α, VEGF-A, IL-10, MCP-1) were sampled across a range from 0.1 to 10 times the calibrated value while holding the other parameters constant. Three hundred samples were generated, and these parameter sets were simulated in triplicate. PRCCs were calculated with α=0.05 and a Bonferroni correction for the number of tests every 10 ticks/hr for CSA and cell counts

Table 9. Summary of cytokine sensitivity analysis.
Significance was determined with α=0.05, and a Bonferroni correction for the number of tests. + and - represent statistically significant positive and negative correlations, respectively.

	CSA	SSC	Fibroblasts	Non-perfused capillaries	Myoblasts	Myocytes	Neutrophils	M1	M2
Day	16.7	6.3	10.5	8.4	6.3	8.4	8.4	4.2	6.3
HGF decay	-	-	-	+	-	-	+		+
TGF-β decay	+	+	+	-	+				-
MMP-9 decay	+	+	+	-	+	+			
TNF-α decay			+						-
VEGF-A decay				+					
MCP-1 decay								+	+
MCP-1 diffusion		+		-				+	

for SSCs, fibroblasts, non-perfused capillaries, myoblasts, myocytes, neutrophils, M1 macrophages, and M2 macrophages.

In silico experiments

To gain insight into the recovery response with altered angiogenesis, we simulated different levels of VEGF-A injections to test how increases in VEGF-A impacted regeneration outcomes. In addition, we simulated conditions of hindered angiogenesis in which damaged capillaries were unable to reperfuse following injury (n=100 for each simulation condition). Simulations were also conducted to examine correlations between cytokines and their impact on various cell behaviors and regeneration outcomes. Next, a sensitivity analysis was performed to understand how alterations in cytokines influence key metrics of regeneration. LHS-PRCC was used to quantify the impact of cytokine-related parameters (i.e. diffusion rates and decay coefficients) on outputs of interest (CSA, SSC, fibroblasts, non-perfused capillaries, myoblasts, myocytes, neutrophils, M1, and M2). A single timepoint for each output is summarized in ***Table 9***, and these were chosen at the timepoint when PRCC values were peaking, with complete results available in ***Figure 6—figure supplement 1***.

This sensitivity analysis was then used to guide in silico experiments based on which cytokine parameters promoted favorable regeneration outcomes (i.e. improved recovery, fewer non-perfused capillaries, increased SSCs). Following individual cytokine parameter alterations, we combined the cytokine alterations based on beneficial outcomes from the initial in silico experiments to determine if the benefits would be cumulative.

Acknowledgements

The authors acknowledge NIH Grant #R21AR080415, Wu-Tsai Foundation Agility Project Funding, and NSF GRFP Grant #1842490 for financially supporting this research and to James Glazier and TJ Sego for providing technical support with the CC3D ABM platform.

Additional information

Funding

Funder	Grant reference number	Author
National Institutes of Health	R21AR080415	Silvia S Blemker
National Science Foundation	1842490	Megan Haase
Wu-Tsai Foundation	Agility Project Funding	Silvia S Blemker

Funder	Grant reference number	Author

The funders had no role in study design, data collection and interpretation, or the decision to submit the work for publication.

Author contributions

Megan Haase, Conceptualization, Data curation, Software, Formal analysis, Funding acquisition, Validation, Investigation, Visualization, Methodology, Writing - original draft, Project administration, Writing – review and editing; Tien Comlekoglu, Data curation, Software, Formal analysis, Investigation, Methodology, Writing - original draft, Writing – review and editing; Alexa Petrucciani, Software, Formal analysis, Investigation, Methodology, Writing - original draft, Writing – review and editing; Shayn M Peirce, Resources, Funding acquisition, Investigation, Methodology, Writing – review and editing; Silvia S Blemker, Conceptualization, Resources, Supervision, Funding acquisition, Investigation, Methodology, Writing – review and editing

Author ORCIDs

Megan Haase http://orcid.org/0000-0002-5221-4495
Shayn M Peirce http://orcid.org/0000-0001-5857-5606
Silvia S Blemker https://orcid.org/0000-0002-2019-1153

Peer review material

Reviewer #1 (Public Review): https://doi.org/10.7554/eLife.91924.3.sa1
Reviewer #2 (Public Review): https://doi.org/10.7554/eLife.91924.3.sa2
Author response https://doi.org/10.7554/eLife.91924.3.sa3

Additional files

Supplementary files

- Supplementary file 1. Unknown model parameters calibrated using Latin hypercube sampling (LHS) to recapitulate published literature.
- Supplementary file 2. Cytokine perturbations based on partial rank correlation coefficient (PRCC).
- Supplementary file 3. Cellular-Potts model (CPM) mathematical implementation.
- Supplementary file 4. Cellular-Potts model (CPM) agent adhesion parameters.
- Supplementary file 5. Cellular-Potts model (CPM) initialization model parameters.
- Supplementary file 6. Criteria utilized for CaliPro model calibration.
- Supplementary file 7. Experimental data description for model comparison.
- MDAR checklist

Data availability

The ABM source code is publicly available at the following sites: SimTK; Zendo; GitHub (copy archived at ***mh2uk, 2024***).

The following datasets were generated:

Author(s)	Year	Dataset title	Dataset URL	Database and Identifier
Haase M, Petrucciani A, Comlekoglu T, Peirce S, Blemker S	2024	Agent-Based Model of Muscle Regeneration with Microvascular Remodeling	https://zenodo.org/doi/10.5281/zenodo.10403013	Zenodo, 10.5281/zenodo.10403013
Haase M, Petrucciani A, Comlekoglu T, Peirce S, Blemker S	2024	Agent-Based Model of Muscle Regeneration with Microvascular Remodeling	https://simtk.org/docman/?group_id=2635	SimTK, 2635

References

Abmayr SM, Pavlath GK. 2012. Myoblast fusion: lessons from flies and mice. *Development* **139**:641–656. DOI: https://doi.org/10.1242/dev.068353, PMID: 22274696

Akhurst RJ. 2002. TGF-beta antagonists: why suppress a tumor suppressor? *The Journal of Clinical Investigation* **109**:1533–1536. DOI: https://doi.org/10.1172/JCI15970, PMID: 12070299

Alberts B, Johnson A, Lewis J, Raff M, Roberts K, Walter P. 2002. Extracellular control of cell division, cell growth, and apoptosis. https://www.ncbi.nlm.nih.gov/books/NBK26877 [Accessed March 13, 2023].

Allen RE, Boxhorn LK. 1989. Regulation of skeletal muscle satellite cell proliferation and differentiation by transforming growth factor-beta, insulin-like growth factor I, and fibroblast growth factor. *Journal of Cellular Physiology* **138**:311–315. DOI: https://doi.org/10.1002/jcp.1041380213, PMID: 2918032

Allen RE, Sheehan SM, Taylor RG, Kendall TL, Rice GM. 1995. Hepatocyte growth factor activates quiescent skeletal muscle satellite cells in vitro. *Journal of Cellular Physiology* **165**:307–312. DOI: https://doi.org/10.1002/jcp.1041650211, PMID: 7593208

Alsousou J, Ali A, Willett K, Harrison P. 2013. The role of platelet-rich plasma in tissue regeneration. *Platelets* **24**:173–182. DOI: https://doi.org/10.3109/09537104.2012.684730, PMID: 22647081

Arabpour M, Saghazadeh A, Rezaei N. 2021. Anti-inflammatory and M2 macrophage polarization-promoting effect of mesenchymal stem cell-derived exosomes. *International Immunopharmacology* **97**:107823. DOI: https://doi.org/10.1016/j.intimp.2021.107823, PMID: 34102486

Arnold L, Henry A, Poron F, Baba-Amer Y, van Rooijen N, Plonquet A, Gherardi RK, Chazaud B. 2007. Inflammatory monocytes recruited after skeletal muscle injury switch into antiinflammatory macrophages to support myogenesis. *The Journal of Experimental Medicine* **204**:1057–1069. DOI: https://doi.org/10.1084/jem.20070075, PMID: 17485518

Arsic N, Zacchigna S, Zentilin L, Ramirez-Correa G, Pattarini L, Salvi A, Sinagra G, Giacca M. 2004. Vascular endothelial growth factor stimulates skeletal muscle regeneration in vivo. *Molecular Therapy* **10**:844–854. DOI: https://doi.org/10.1016/j.ymthe.2004.08.007, PMID: 15509502

Bakkar N, Wang J, Ladner KJ, Wang H, Dahlman JM, Carathers M, Acharyya S, Rudnicki MA, Hollenbach AD, Guttridge DC. 2008. IKK/NF-kappaB regulates skeletal myogenesis via a signaling switch to inhibit differentiation and promote mitochondrial biogenesis. *The Journal of Cell Biology* **180**:787–802. DOI: https://doi.org/10.1083/jcb.200707179, PMID: 18299349

Barroso GC, Thiele ES. 2011. Muscle injuries in athletes. *Revista Brasileira de Ortopedia* **46**:354–358. DOI: https://doi.org/10.1016/S2255-4971(15)30245-7

Beanes SR, Dang C, Soo C, Ting K. 2003. Skin repair and scar formation: the central role of TGF-β. *Expert Reviews in Molecular Medicine* **5**:1–22. DOI: https://doi.org/10.1017/S1462399403005817

Bentzinger CF, Wang YX, Rudnicki MA. 2012. Building muscle: molecular regulation of myogenesis. *Cold Spring Harbor Perspectives in Biology* **4**:a008342. DOI: https://doi.org/10.1101/cshperspect.a008342, PMID: 22300977

Butterfield TA, Best TM, Merrick MA. 2006. The dual roles of neutrophils and macrophages in inflammation: a critical balance between tissue damage and repair. *Journal of Athletic Training* **41**:457–465. DOI: https://doi.org/10.1016/s0162-0908(08)79217-1, PMID: 17273473

Cantaert T, Baeten D, Tak PP, van Baarsen LGM. 2010. Type I IFN and TNFα cross-regulation in immune-mediated inflammatory disease: basic concepts and clinical relevance. *Arthritis Research & Therapy* **12**:219. DOI: https://doi.org/10.1186/ar3150, PMID: 21062511

Cencetti F, Bernacchioni C, Tonelli F, Roberts E, Donati C, Bruni P. 2013. TGFβ1 evokes myoblast apoptotic response via a novel signaling pathway involving S1P4 transactivation upstream of Rho-kinase-2 activation. *FASEB Journal* **27**:4532–4546. DOI: https://doi.org/10.1096/fj.13-228528, PMID: 23913862

Chazaud B, Sonnet C, Lafuste P, Bassez G, Rimaniol A-C, Poron F, Authier F-J, Dreyfus PA, Gherardi RK. 2003. Satellite cells attract monocytes and use macrophages as a support to escape apoptosis and enhance muscle growth. *The Journal of Cell Biology* **163**:1133–1143. DOI: https://doi.org/10.1083/jcb.200212046, PMID: 14662751

Chellini F, Tani A, Zecchi-Orlandini S, Sassoli C. 2019. Influence of platelet-rich and platelet-poor plasma on endogenous mechanisms of skeletal muscle repair/regeneration. *International Journal of Molecular Sciences* **20**:683. DOI: https://doi.org/10.3390/ijms20030683, PMID: 30764506

Chen S-E, Gerken E, Zhang Y, Zhan M, Mohan RK, Li AS, Reid MB, Li Y-P. 2005. Role of TNF-{alpha} signaling in regeneration of cardiotoxin-injured muscle. *American Journal of Physiology. Cell Physiology* **289**:C1179–C1187. DOI: https://doi.org/10.1152/ajpcell.00062.2005, PMID: 16079187

Chen X, Li Y. 2009. Role of matrix metalloproteinases in skeletal muscle: migration, differentiation, regeneration and fibrosis. *Cell Adhesion & Migration* **3**:337–341. DOI: https://doi.org/10.4161/cam.3.4.9338, PMID: 19667757

Chen GY, Nuñez G. 2010. Sterile inflammation: sensing and reacting to damage. *Nature Reviews. Immunology* **10**:826–837. DOI: https://doi.org/10.1038/nri2873, PMID: 21088683

Chen CH, Chang CH, Lee CH. 2015. Usage of growth factors in acute muscle injuries. Doral MN, Karlsson J (Eds). *Sports Injuries*. Springer. p. 2343–2351. DOI: https://doi.org/10.1007/978-3-642-36569-0_174

Choi W, Lee J, Lee J, Lee SH, Kim S. 2019. Hepatocyte Growth Factor Regulates Macrophage Transition to the M2 Phenotype and Promotes Murine Skeletal Muscle Regeneration. *Frontiers in Physiology* **10**:914. DOI: https://doi.org/10.3389/fphys.2019.00914, PMID: 31404148

Chung EY, Liu J, Homma Y, Zhang Y, Brendolan A, Saggese M, Han J, Silverstein R, Selleri L, Ma X. 2007. Interleukin-10 expression in macrophages during phagocytosis of apoptotic cells is mediated by homeodomain proteins Pbx1 and Prep-1. *Immunity* **27**:952–964. DOI: https://doi.org/10.1016/j.immuni.2007.11.014, PMID: 18093541

Ciano-Petersen NL, Muñiz-Castrillo S, Birzu C, Vogrig A, Farina A, Villagrán-García M, Joubert B, Psimaras D, Honnorat J. 2022. Cytokine dynamics and targeted immunotherapies in autoimmune encephalitis. *Brain Communications* **4**:fcac196. DOI: https://doi.org/10.1093/braincomms/fcac196, PMID: 35999839

Cooper RN, Tajbakhsh S, Mouly V, Cossu G, Buckingham M, Butler-Browne GS. 1999. In vivo satellite cell activation via Myf5 and MyoD in regenerating mouse skeletal muscle. *Journal of Cell Science* **112 (Pt 17)**:2895–2901. DOI: https://doi.org/10.1242/jcs.112.17.2895, PMID: 10444384

Corliss BA, Azimi MS, Munson JM, Peirce SM, Murfee WL. 2016. Macrophages: an inflammatory link between angiogenesis and lymphangiogenesis. *Microcirculation* **23**:95–121. DOI: https://doi.org/10.1111/micc.12259, PMID: 26614117

Cornwell KG, Downing BR, Pins GD. 2004. Characterizing fibroblast migration on discrete collagen threads for applications in tissue regeneration. *Journal of Biomedical Materials Research. Part A* **71**:55–62. DOI: https://doi.org/10.1002/jbm.a.30132, PMID: 15368254

Cui K, Ardell CL, Podolnikova NP, Yakubenko VP. 2018. Distinct Migratory Properties of M1, M2, and Resident Macrophages Are Regulated by αDβ2 and αMβ2 Integrin-Mediated Adhesion. *Frontiers in Immunology* **9**:02650. DOI: https://doi.org/10.3389/fimmu.2018.02650

D'Angelo F, Bernasconi E, Schäfer M, Moyat M, Michetti P, Maillard MH, Velin D. 2013. Macrophages promote epithelial repair through hepatocyte growth factor secretion. *Clinical and Experimental Immunology* **174**:60–72. DOI: https://doi.org/10.1111/cei.12157, PMID: 23773083

Das A, Sinha M, Datta S, Abas M, Chaffee S, Sen CK, Roy S. 2015. Monocyte and macrophage plasticity in tissue repair and regeneration. *The American Journal of Pathology* **185**:2596–2606. DOI: https://doi.org/10.1016/j.ajpath.2015.06.001, PMID: 26118749

da Silva MD, Bobinski F, Sato KL, Kolker SJ, Sluka KA, Santos ARS. 2015. IL-10 Cytokine Released from M2 Macrophages Is Crucial for Analgesic and Anti-inflammatory Effects of Acupuncture in a Model of Inflammatory Muscle Pain. *Molecular Neurobiology* **51**:19–31. DOI: https://doi.org/10.1007/s12035-014-8790-x

Deng B, Wehling-Henricks M, Villalta SA, Wang Y, Tidball JG. 2012. IL-10 triggers changes in macrophage phenotype that promote muscle growth and regeneration. *Journal of Immunology* **189**:3669–3680. DOI: https://doi.org/10.4049/jimmunol.1103180, PMID: 22933625

Desmoulière A, Geinoz A, Gabbiani F, Gabbiani G. 1993. Transforming growth factor-beta 1 induces alpha-smooth muscle actin expression in granulation tissue myofibroblasts and in quiescent and growing cultured fibroblasts. *The Journal of Cell Biology* **122**:103–111. DOI: https://doi.org/10.1083/jcb.122.1.103, PMID: 8314838

Dickinson RB, Guido S, Tranquillo RT. 1994. Biased cell migration of fibroblasts exhibiting contact guidance in oriented collagen gels. *Annals of Biomedical Engineering* **22**:342–356. DOI: https://doi.org/10.1007/BF02368241, PMID: 7998680

Downey GP, Doherty DE, Schwab B, Elson EL, Henson PM, Worthen GS. 1990. Retention of leukocytes in capillaries: role of cell size and deformability. *Journal of Applied Physiology* **69**:1767–1778. DOI: https://doi.org/10.1152/jappl.1990.69.5.1767, PMID: 2272970

Dziki JL, Velayutham M, Hussey GS, Turnquist HR. 2018. Cytokine networks in immune-mediated muscle regeneration. *Journal of Immunology and Regenerative Medicine* **1**:32–44. DOI: https://doi.org/10.1016/j.regen.2018.03.001

Elkington PT, Green JA, Friedland JS. 2009. Analysis of matrix metalloproteinase secretion by macrophages. *Methods in Molecular Biology* **531**:253–265. DOI: https://doi.org/10.1007/978-1-59745-396-7_16, PMID: 19347322

Enns DL, Tiidus PM. 2010. The Influence of Estrogen on Skeletal Muscle. *Sports Medicine* **40**:41–58. DOI: https://doi.org/10.2165/11319760-000000000-00000

ExternalPotential Plugin. 2024. ExternalPotential Plugin — CC3D Reference Manual 4.4.1 documentation. https://compucell3dreferencemanual.readthedocs.io/en/latest/external_potential_plugin.html [Accessed January 4, 2024].

Ferrara N. 2010. Binding to the extracellular matrix and proteolytic processing: two key mechanisms regulating vascular endothelial growth factor action. *Molecular Biology of the Cell* **21**:687–690. DOI: https://doi.org/10.1091/mbc.e09-07-0590, PMID: 20185770

Ferrari Gianlupi J, Mapder T, Sego TJ, Sluka JP, Quinney SK, Craig M, Stratford RE, Glazier JA. 2022. Multiscale model of antiviral timing, potency, and heterogeneity effects on an epithelial tissue patch infected by SARS-CoV-2. *Viruses* **14**:605. DOI: https://doi.org/10.3390/v14030605, PMID: 35337012

Filion RJ, Popel AS. 2005. Intracoronary administration of FGF-2: A computational model of myocardial deposition and retention. *American Journal of Physiology-Heart and Circulatory Physiology* **288**:H263–H279. DOI: https://doi.org/10.1152/ajpheart.00205.2004

Flamini V, Ghadiali RS, Antczak P, Rothwell A, Turnbull JE, Pisconti A. 2018. The satellite cell niche regulates the balance between myoblast differentiation and self-renewal via p53. *Stem Cell Reports* **10**:970–983. DOI: https://doi.org/10.1016/j.stemcr.2018.01.007, PMID: 29429962

Forcina L, Cosentino M, Musarò A. 2020. Mechanisms regulating muscle regeneration: insights into the interrelated and time-dependent phases of tissue healing. *Cells* **9**:1297. DOI: https://doi.org/10.3390/cells9051297, PMID: 32456017

Fox S, Leitch AE, Duffin R, Haslett C, Rossi AG. 2010. Neutrophil apoptosis: relevance to the innate immune response and inflammatory disease. *Journal of Innate Immunity* **2**:216–227. DOI: https://doi.org/10.1159/000284367, PMID: 20375550

Freitas RJ. 1999. Nanomedicine: basic capabilities. http://www.nanomedicine.com/NMI/8.5.1.htm [Accessed May 16, 2022].
Frey SP, Jansen H, Raschke MJ, Meffert RH, Ochman S. 2012. VEGF improves skeletal muscle regeneration after acute trauma and reconstruction of the limb in a rabbit model. *Clinical Orthopaedics and Related Research* **470**:3607–3614. DOI: https://doi.org/10.1007/s11999-012-2456-7, PMID: 22806260
Fujita R, Kawano F, Ohira T, Nakai N, Shibaguchi T, Nishimoto N, Ohira Y. 2014. Anti-interleukin-6 receptor antibody (MR16-1) promotes muscle regeneration via modulation of gene expressions in infiltrated macrophages. *Biochimica et Biophysica Acta* **1840**:3170–3180. DOI: https://doi.org/10.1016/j.bbagen.2014.01.014
Furrer R, Handschin C. 2017. Optimized engagement of Macrophages and satellite cells in the repair and regeneration of exercised muscle. Spiegelman B (Ed). *Research and Perspectives in Endocrine Interactions*. Springer. p. 57–66. DOI: https://doi.org/10.1007/978-3-319-72790-5
Gal-Levi R, Leshem Y, Aoki S, Nakamura T, Halevy O. 1998. Hepatocyte growth factor plays a dual role in regulating skeletal muscle satellite cell proliferation and differentiation. *Biochimica et Biophysica Acta* **1402**:39–51. DOI: https://doi.org/10.1016/S0167-4889(97)00124-9
Garcia SM, Tamaki S, Lee S, Wong A, Jose A, Dreux J, Kouklis G, Sbitany H, Seth R, Knott PD, Heaton C, Ryan WR, Kim EA, Hansen SL, Hoffman WY, Pomerantz JH. 2018. High-yield purification, preservation, and serial transplantation of human satellite cells. *Stem Cell Reports* **10**:1160–1174. DOI: https://doi.org/10.1016/j.stemcr.2018.01.022
Gehlert S, Theis C, Weber S, Schiffer T, Hellmich M, Platen P, Bloch W. 2010. Exercise-induced decline in the density of LYVE-1-positive lymphatic vessels in human skeletal muscle. *Lymphatic Research and Biology* **8**:165–173. DOI: https://doi.org/10.1089/lrb.2009.0035, PMID: 20863269
Gibb AA, Lazaropoulos MP, Elrod JW. 2020. Myofibroblasts and Fibrosis. *Circulation Research* **127**:427–447. DOI: https://doi.org/10.1161/CIRCRESAHA.120.316958
Girardi F, Taleb A, Ebrahimi M, Datye A, Gamage DG, Peccate C, Giordani L, Millay DP, Gilbert PM, Cadot B, Le Grand F. 2021. TGFβ signaling curbs cell fusion and muscle regeneration. *Nature Communications* **12**:750. DOI: https://doi.org/10.1038/s41467-020-20289-8, PMID: 33531466
González MN, de Mello W, Butler-Browne GS, Silva-Barbosa SD, Mouly V, Savino W, Riederer I. 2017. HGF potentiates extracellular matrix-driven migration of human myoblasts: involvement of matrix metalloproteinases and MAPK/ERK pathway. *Skeletal Muscle* **7**:20. DOI: https://doi.org/10.1186/s13395-017-0138-6, PMID: 29017538
Greenlee-Wacker MC. 2016. Clearance of apoptotic neutrophils and resolution of inflammation. *Immunological Reviews* **273**:357–370. DOI: https://doi.org/10.1111/imr.12453, PMID: 27558346
Haas TL, Milkiewicz M, Davis SJ, Zhou AL, Egginton S, Brown MD, Madri JA, Hudlicka O. 2000. Matrix metalloproteinase activity is required for activity-induced angiogenesis in rat skeletal muscle. *American Journal of Physiology. Heart and Circulatory Physiology* **279**:H1540–H1547. DOI: https://doi.org/10.1152/ajpheart.2000.279.4.H1540, PMID: 11009439
Haizlip KM, Harrison BC, Leinwand LA. 2015. Sex-based differences in skeletal muscle kinetics and fiber-type composition. *Physiology* **30**:30–39. DOI: https://doi.org/10.1152/physiol.00024.2014, PMID: 25559153
Hampton HR, Chtanova T. 2019. Lymphatic migration of immune cells. *Frontiers in Immunology* **10**:1168. DOI: https://doi.org/10.3389/fimmu.2019.01168, PMID: 31191539
Hardy D, Besnard A, Latil M, Jouvion G, Briand D, Thépenier C, Pascal Q, Guguin A, Gayraud-Morel B, Cavaillon J-M, Tajbakhsh S, Rocheteau P, Chrétien F. 2016. Comparative study of injury models for studying muscle regeneration in mice. *PLOS ONE* **11**:e0147198. DOI: https://doi.org/10.1371/journal.pone.0147198, PMID: 26807982
Hardy D, Fefeu M, Besnard A, Briand D, Gasse P, Arenzana-Seisdedos F, Rocheteau P, Chrétien F. 2019. Defective angiogenesis in CXCL12 mutant mice impairs skeletal muscle regeneration. *Skeletal Muscle* **9**:25. DOI: https://doi.org/10.1186/s13395-019-0210-5, PMID: 31533830
Heit B, Liu L, Colarusso P, Puri KD, Kubes P. 2008. PI3K accelerates, but is not required for, neutrophil chemotaxis to fMLP. *Journal of Cell Science* **121**:205–214. DOI: https://doi.org/10.1242/jcs.020412
Howard EE, Pasiakos SM, Blesso CN, Fussell MA, Rodriguez NR. 2020. Divergent roles of inflammation in skeletal muscle recovery from injury. *Frontiers in Physiology* **11**:87. DOI: https://doi.org/10.3389/fphys.2020.00087, PMID: 32116792
Huard J, Li Y, Fu FH. 2022. Muscle injuries and repair: Current trends in research. *J Bone Jt Surg* **01**:00022. DOI: https://doi.org/10.2106/00004623-200205000-00022
Huey KA. 2018. Potential roles of vascular endothelial growth factor during skeletal muscle hypertrophy. *Exercise and Sport Sciences Reviews* **46**:195–202. DOI: https://doi.org/10.1249/JES.0000000000000152, PMID: 29652692
Husmann I, Soulet L, Gautron J, Martelly I, Barritault D. 1996. Growth factors in skeletal muscle regeneration. *Cytokine & Growth Factor Reviews* **7**:249–258. DOI: https://doi.org/10.1016/s1359-6101(96)00029-9, PMID: 8971480
Isesele PO, Mazurak VC. 2021. Regulation of skeletal muscle satellite cell differentiation by Omega-3 polyunsaturated fatty acids: A critical review. *Frontiers in Physiology* **12**:682091. DOI: https://doi.org/10.3389/fphys.2021.682091, PMID: 34149458
Ismail AA, Shaker BT, Bajou K. 2021. The plasminogen-activator plasmin system in physiological and pathophysiological angiogenesis. *International Journal of Molecular Sciences* **23**:337. DOI: https://doi.org/10.3390/ijms23010337, PMID: 35008762

Itoh Y. 2022. Proteolytic modulation of tumor microenvironment signals during cancer progression. *Frontiers in Oncology* **12**:935231. DOI: https://doi.org/10.3389/fonc.2022.935231, PMID: 36132127

Jacobsen NL, Norton CE, Shaw RL, Cornelison D, Segal SS. 2021. Myofiber injury induces capillary disruption and regeneration of disorganized microvascular networks. *bioRxiv*. DOI: https://doi.org/10.1101/2021.08.02.454805

Järvinen TAH, Järvinen TLN, Kääriäinen M, Aärimaa V, Vaittinen S, Kalimo H, Järvinen M. 2007. Muscle injuries: optimising recovery. *Best Practice & Research. Clinical Rheumatology* **21**:317–331. DOI: https://doi.org/10.1016/j.berh.2006.12.004, PMID: 17512485

Joslyn LR, Kirschner DE, Linderman JJ. 2021. *CaliPro*: a calibration protocol that utilizes parameter density estimation to explore parameter space and calibrate complex biological models. *Cellular and Molecular Bioengineering* **14**:31–47. DOI: https://doi.org/10.1007/s12195-020-00650-z, PMID: 33643465

Kawamura K, Takano K, Suetsugu S, Kurisu S, Yamazaki D, Miki H, Takenawa T, Endo T. 2004. N-WASP and WAVE2 acting downstream of phosphatidylinositol 3-kinase are required for myogenic cell migration induced by hepatocyte growth factor. *The Journal of Biological Chemistry* **279**:54862–54871. DOI: https://doi.org/10.1074/jbc.M408057200, PMID: 15496413

Khuu S, Fernandez JW, Handsfield GG. 2021. A coupled mechanobiological model of muscle regeneration in cerebral palsy. *Frontiers in Bioengineering and Biotechnology* **9**:689714. DOI: https://doi.org/10.3389/fbioe.2021.689714, PMID: 34513808

Khuu S, Fernandez JW, Handsfield GG, ed. 2023. Delayed skeletal muscle repair following inflammatory damage in simulated agent-based models of muscle regeneration. *PLOS Computational Biology* **19**:e1011042. DOI: https://doi.org/10.1371/journal.pcbi.1011042

Kim J, Lee J. 2017. Role of transforming growth factor-β in muscle damage and regeneration: focused on eccentric muscle contraction. *Journal of Exercise Rehabilitation* **13**:621–626. DOI: https://doi.org/10.12965/jer.1735072.536, PMID: 29326892

Knewtson KE, Ohl NR, Robinson JL. 2022. Estrogen signaling dictates musculoskeletal stem cell behavior: sex differences in tissue repair. *Tissue Engineering Part B* **28**:789–812. DOI: https://doi.org/10.1089/ten.teb.2021.0094

Kratofil RM, Kubes P, Deniset JF. 2017. Monocyte conversion during inflammation and injury. *Arteriosclerosis, Thrombosis, and Vascular Biology* **37**:35–42. DOI: https://doi.org/10.1161/ATVBAHA.116.308198, PMID: 27765768

Krombach F, Münzing S, Allmeling AM, Gerlach JT, Behr J, Dörger M. 1997. Cell size of alveolar macrophages: an interspecies comparison. *Environmental Health Perspectives* **105 Suppl 5**:1261–1263. DOI: https://doi.org/10.1289/ehp.97105s51261, PMID: 9400735

Kuang S, Kuroda K, Le Grand F, Rudnicki MA. 2007. Asymmetric self-renewal and commitment of satellite stem cells in muscle. *Cell* **129**:999–1010. DOI: https://doi.org/10.1016/j.cell.2007.03.044, PMID: 17540178

Kunze KN, Hannon CP, Fialkoff JD, Frank RM, Cole BJ. 2019. Platelet-rich plasma for muscle injuries: A systematic review of the basic science literature. *World Journal of Orthopedics* **10**:278–291. DOI: https://doi.org/10.5312/wjo.v10.i7.278, PMID: 31363458

Lacy P, Stow JL. 2011. Cytokine release from innate immune cells: association with diverse membrane trafficking pathways. *Blood* **118**:9–18. DOI: https://doi.org/10.1182/blood-2010-08-265892, PMID: 21562044

Lemos DR, Babaeijandaghi F, Low M, Chang C-K, Lee ST, Fiore D, Zhang R-H, Natarajan A, Nedospasov SA, Rossi FMV. 2015. Nilotinib reduces muscle fibrosis in chronic muscle injury by promoting TNF-mediated apoptosis of fibro/adipogenic progenitors. *Nature Medicine* **21**:786–794. DOI: https://doi.org/10.1038/nm.3869, PMID: 26053624

Li H, Mittal A, Makonchuk DY, Bhatnagar S, Kumar A. 2009. Matrix metalloproteinase-9 inhibition ameliorates pathogenesis and improves skeletal muscle regeneration in muscular dystrophy. *Human Molecular Genetics* **18**:2584–2598. DOI: https://doi.org/10.1093/hmg/ddp191

Lin CC, Boyer PD, Aimetti AA, Anseth KS. 2010. Regulating MCP-1 diffusion in affinity hydrogels for enhancing immuno-isolation. *Journal of Controlled Release* **142**:384–391. DOI: https://doi.org/10.1016/j.jconrel.2009.11.022

Lindner D, Zietsch C, Becher PM, Schulze K, Schultheiss H-P, Tschöpe C, Westermann D. 2012. Differential expression of matrix metalloproteases in human fibroblasts with different origins. *Biochemistry Research International* **2012**:875742. DOI: https://doi.org/10.1155/2012/875742, PMID: 22500233

Liu X, Liu Y, Zhao L, Zeng Z, Xiao W, Chen P. 2017. Macrophage depletion impairs skeletal muscle regeneration: The roles of regulatory factors for muscle regeneration. *Cell Biology International* **41**:228–238. DOI: https://doi.org/10.1002/cbin.10705, PMID: 27888539

Liu S, Kostek M, Omstead K. 2023. Sex based differences in muscle regeneration. *Physiology* **38**:5729941. DOI: https://doi.org/10.1152/physiol.2023.38.S1.5729941

Lu H, Huang D, Ransohoff RM, Zhou L. 2011. Acute skeletal muscle injury: CCL2 expression by both monocytes and injured muscle is required for repair. *FASEB Journal* **25**:3344–3355. DOI: https://doi.org/10.1096/fj.10-178939, PMID: 21697550

Lu HL, Huang XY, Luo YF, Tan WP, Chen PF, Guo YB. 2018. Activation of M1 macrophages plays a critical role in the initiation of acute lung injury. *Bioscience Reports* **38**:20171555. DOI: https://doi.org/10.1042/BSR20171555

Madaro L, Bouché M. 2014. From innate to adaptive immune response in muscular dystrophies and skeletal muscle regeneration: the role of lymphocytes. *BioMed Research International* **2014**:438675. DOI: https://doi.org/10.1155/2014/438675, PMID: 25028653

Marino S, Hogue IB, Ray CJ, Kirschner DE. 2008. A methodology for performing global uncertainty and sensitivity analysis in systems biology. *Journal of Theoretical Biology* **254**:178–196. DOI: https://doi.org/10.1016/j.jtbi.2008.04.011, PMID: 18572196

Marino S, Hult C, Wolberg P, Linderman JJ, Kirschner DE. 2018. The role of dimensionality in understanding granuloma formation. *Computation* **6**:58. DOI: https://doi.org/10.3390/computation6040058, PMID: 31258937

Martin KS, Blemker SS, Peirce SM. 2015. Agent-based computational model investigates muscle-specific responses to disuse-induced atrophy. *Journal of Applied Physiology* **118**:1299–1309. DOI: https://doi.org/10.1152/japplphysiol.01150.2014, PMID: 25722379

Martin KS, Virgilio KM, Peirce SM, Blemker SS. 2016. Computational modeling of muscle regeneration and adaptation to advance muscle tissue regeneration strategies. *Cells Tissues Organs* **202**:250–266. DOI: https://doi.org/10.1159/000443635

Martin KS, Kegelman CD, Virgilio KM, Passipieri JA, Christ GJ, Blemker SS, Peirce SM. 2017. In silico and in vivo experiments reveal M-CSF injections accelerate regeneration following muscle laceration. *Annals of Biomedical Engineering* **45**:747–760. DOI: https://doi.org/10.1007/s10439-016-1707-2

mh2uk. 2024. ABM-of-muscle-regeneration-with-Microvascular-remodeling. swh:1:rev:41a23b0ff07bc41d1eb01b87432714c28b77950e. Software Heritage. https://archive.softwareheritage.org/swh:1:dir:d4d4421de42509c97f52053c41d6df9c968bcd3e;origin=https://github.com/mh2uk/ABM-of-Muscle-Regeneration-with-Microvascular-Remodeling;visit=swh:1:snp:03214446d9997d16d097d46cc08f0f983f29da47;anchor=swh:1:rev:41a23b0ff07bc41d1eb01b87432714c28b77950e

Miller KJ, Thaloor D, Matteson S, Pavlath GK. 2000. Hepatocyte growth factor affects satellite cell activation and differentiation in regenerating skeletal muscle. *American Journal of Physiology. Cell Physiology* **278**:C174–C181. DOI: https://doi.org/10.1152/ajpcell.2000.278.1.C174, PMID: 10644525

Molnarfi N, Benkhoucha M, Funakoshi H, Nakamura T, Lalive PH. 2015. Hepatocyte growth factor: a regulator of inflammation and autoimmunity. *Autoimmunity Reviews* **14**:293–303. DOI: https://doi.org/10.1016/j.autrev.2014.11.013, PMID: 25476732

Moncayo AR. 2007. Poisson convergence and family trees. *The Annals of Probability* **3**:1176996235. DOI: https://doi.org/10.1214/aop/1176996235

Mosser DM, Edwards JP. 2008. Exploring the full spectrum of macrophage activation. *Nature Reviews. Immunology* **8**:958–969. DOI: https://doi.org/10.1038/nri2448, PMID: 19029990

Murphy MM, Lawson JA, Mathew SJ, Hutcheson DA, Kardon G. 2011. Satellite cells, connective tissue fibroblasts and their interactions are crucial for muscle regeneration. *Development* **138**:3625–3637. DOI: https://doi.org/10.1242/dev.064162, PMID: 21828091

Newby AC. 2008. Metalloproteinase expression in monocytes and macrophages and its relationship to atherosclerotic plaque instability. *Arteriosclerosis, Thrombosis, and Vascular Biology* **28**:2108–2114. DOI: https://doi.org/10.1161/ATVBAHA.108.173898

Newman AC, Nakatsu MN, Chou W, Gershon PD, Hughes CCW. 2011. The requirement for fibroblasts in angiogenesis: fibroblast-derived matrix proteins are essential for endothelial cell lumen formation. *Molecular Biology of the Cell* **22**:3791–3800. DOI: https://doi.org/10.1091/mbc.E11-05-0393, PMID: 21865599

Nguyen MH, Cheng M, Koh TJ. 2011. Impaired muscle regeneration in ob/ob and db/db mice. *TheScientificWorldJournal* **11**:1525–1535. DOI: https://doi.org/10.1100/tsw.2011.137, PMID: 21805021

Nguyen JH, Chung JD, Lynch GS, Ryall JG. 2019. The microenvironment is a critical regulator of muscle stem cell activation and proliferation. *Frontiers in Cell and Developmental Biology* **7**:254. DOI: https://doi.org/10.3389/fcell.2019.00254, PMID: 31737625

Ochoa O, Sun D, Reyes-Reyna SM, Waite LL, Michalek JE, McManus LM, Shireman PK. 2007. Delayed angiogenesis and VEGF production in CCR2−/− mice during impaired skeletal muscle regeneration. *American Journal of Physiology-Regulatory, Integrative and Comparative Physiology* **293**:R651–R661. DOI: https://doi.org/10.1152/ajpregu.00069.2007

Oishi Y, Manabe I. 2018. Macrophages in inflammation, repair and regeneration. *International Immunology* **30**:511–528. DOI: https://doi.org/10.1093/intimm/dxy054, PMID: 30165385

Otto A, Collins-Hooper H, Patel A, Dash PR, Patel K. 2011. Adult skeletal muscle stem cell migration is mediated by a blebbing/amoeboid mechanism. *Rejuvenation Research* **14**:249–260. DOI: https://doi.org/10.1089/rej.2010.1151, PMID: 21453013

Owen JL, Mohamadzadeh M. 2013. Macrophages and chemokines as mediators of angiogenesis. *Frontiers in Physiology* **4**:159. DOI: https://doi.org/10.3389/fphys.2013.00159, PMID: 23847541

Perandini LA, Chimin P, da S Lutkemeyer D, Câmara NOS. 2018. Chronic inflammation in skeletal muscle impairs satellite cells function during regeneration: can physical exercise restore the satellite cell niche? *The FEBS Journal* **285**:1973–1984. DOI: https://doi.org/10.1111/febs.14417, PMID: 29473995

Petrov VV, Fagard RH, Lijnen PJ. 2002. Stimulation of collagen production by transforming growth factor-beta1 during differentiation of cardiac fibroblasts to myofibroblasts. *Hypertension* **39**:258–263. DOI: https://doi.org/10.1161/hy0202.103268, PMID: 11847194

Popov Y, Sverdlov DY, Bhaskar KR, Sharma AK, Millonig G, Patsenker E, Krahenbuhl S, Krahenbuhl L, Schuppan D. 2010. Macrophage-mediated phagocytosis of apoptotic cholangiocytes contributes to reversal of experimental biliary fibrosis. *American Journal of Physiology. Gastrointestinal and Liver Physiology* **298**:G323–G334. DOI: https://doi.org/10.1152/ajpgi.00394.2009, PMID: 20056896

Pratt SJP, Shah SB, Ward CW, Kerr JP, Stains JP, Lovering RM. 2015. Recovery of altered neuromuscular junction morphology and muscle function in mdx mice after injury. *Cellular and Molecular Life Sciences* **72**:153–164. DOI: https://doi.org/10.1007/s00018-014-1663-7, PMID: 24947322

Quintero AJ, Wright VJ, Fu FH, Huard J. 2009. Stem cells for the treatment of skeletal muscle injury. *Clinics in Sports Medicine* **28**:1–11. DOI: https://doi.org/10.1016/j.csm.2008.08.009, PMID: 19064161

Qutub AA, Mac Gabhann F, Karagiannis ED, Vempati P, Popel AS. 2009. Multiscale models of angiogenesis. *IEEE Engineering in Medicine and Biology Magazine* **28**:14–31. DOI: https://doi.org/10.1109/MEMB.2009.931791, PMID: 19349248

Raimondo TM, Mooney DJ. 2018. Functional muscle recovery with nanoparticle-directed M2 macrophage polarization in mice. *PNAS* **115**:10648–10653. DOI: https://doi.org/10.1073/pnas.1806908115, PMID: 30275293

Reibman J, Meixler S, Lee TC, Gold LI, Cronstein BN, Haines KA, Kolasinski SL, Weissmann G. 1991. Transforming growth factor beta 1, a potent chemoattractant for human neutrophils, bypasses classic signal-transduction pathways. *PNAS* **88**:6805–6809. DOI: https://doi.org/10.1073/pnas.88.15.6805, PMID: 1650483

Reimann J, Irintchev A, Wernig A. 2000. Regenerative capacity and the number of satellite cells in soleus muscles of normal and mdx mice. *Neuromuscular Disorders* **10**:276–282. DOI: https://doi.org/10.1016/s0960-8966(99)00118-2, PMID: 10838255

Rocheteau P, Gayraud-Morel B, Siegl-Cachedenier I, Blasco MA, Tajbakhsh S. 2012. A subpopulation of adult skeletal muscle stem cells retains all template DNA Strands after cell division. *Cell* **148**:112–125. DOI: https://doi.org/10.1016/j.cell.2011.11.049

Rucavado A, Escalante T, Teixeira CFP, Fernándes CM, Diaz C, Gutiérrez JM. 2002. Increments in cytokines and matrix metalloproteinases in skeletal muscle after injection of tissue-damaging toxins from the venom of the snake Bothrops asper. *Mediators of Inflammation* **11**:121–128. DOI: https://doi.org/10.1080/09629350220131980, PMID: 12061424

Ruiz-Gómez M, Coutts N, Suster ML, Landgraf M, Bate M. 2002. myoblasts incompetent encodes a zinc finger transcription factor required to specify fusion-competent myoblasts in *Drosophila*. *Development* **129**:133–141. DOI: https://doi.org/10.1242/dev.129.1.133, PMID: 11782407

Saclier M, Yacoub-Youssef H, Mackey AL, Arnold L, Ardjoune H, Magnan M, Sailhan F, Chelly J, Pavlath GK, Mounier R, Kjaer M, Chazaud B. 2013. Differentially activated macrophages orchestrate myogenic precursor cell fate during human skeletal muscle regeneration. *Stem Cells* **31**:384–396. DOI: https://doi.org/10.1002/stem.1288, PMID: 23169615

Saini J, McPhee JS, Al-Dabbagh S, Stewart CE, Al-Shanti N. 2016. Regenerative function of immune system: Modulation of muscle stem cells. *Ageing Research Reviews* **27**:67–76. DOI: https://doi.org/10.1016/j.arr.2016.03.006, PMID: 27039885

Sanderson RD, Fitch JM, Linsenmayer TR, Mayne R. 1986. Fibroblasts promote the formation of a continuous basal lamina during myogenesis in vitro. *The Journal of Cell Biology* **102**:740–747. DOI: https://doi.org/10.1083/jcb.102.3.740, PMID: 3949876

Sego TJ, Kasacheuski U, Hauersperger D, Tovar A, Moldovan NI. 2017. A heuristic computational model of basic cellular processes and oxygenation during spheroid-dependent biofabrication. *Biofabrication* **9**:024104. DOI: https://doi.org/10.1088/1758-5090/aa6ed4, PMID: 28617667

Segovia-Juarez JL, Ganguli S, Kirschner D. 2004. Identifying control mechanisms of granuloma formation during M. tuberculosis infection using an agent-based model. *Journal of Theoretical Biology* **231**:357–376. DOI: https://doi.org/10.1016/j.jtbi.2004.06.031

Siegel AL, Kuhlmann PK, Cornelison DDW. 2011. Muscle satellite cell proliferation and association: new insights from myofiber time-lapse imaging. *Skeletal Muscle* **1**:7. DOI: https://doi.org/10.1186/2044-5040-1-7, PMID: 21798086

Skutek M, van Griensven M, Zeichen J, Brauer N, Bosch U. 2001. Cyclic mechanical stretching modulates secretion pattern of growth factors in human tendon fibroblasts. *European Journal of Applied Physiology* **86**:48–52. DOI: https://doi.org/10.1007/s004210100502, PMID: 11820322

Snijders T, Nederveen JP, McKay BR, Joanisse S, Verdijk LB, van Loon LJC, Parise G. 2015. Satellite cells in human skeletal muscle plasticity. *Frontiers in Physiology* **6**:283. DOI: https://doi.org/10.3389/fphys.2015.00283, PMID: 26557092

Soehnlein O, Zernecke A, Eriksson EE, Rothfuchs AG, Pham CT, Herwald H, Bidzhekov K, Rottenberg ME, Weber C, Lindbom L. 2008. Neutrophil secretion products pave the way for inflammatory monocytes. *Blood* **112**:1461–1471. DOI: https://doi.org/10.1182/blood-2008-02-139634, PMID: 18490516

Sonnet C, Lafuste P, Arnold L, Brigitte M, Poron F, Authier F-J, Chrétien F, Gherardi RK, Chazaud B. 2006. Human macrophages rescue myoblasts and myotubes from apoptosis through a set of adhesion molecular systems. *Journal of Cell Science* **119**:2497–2507. DOI: https://doi.org/10.1242/jcs.02988, PMID: 16720640

Stephenson ER, Kojouharov HV. 2018. A mathematical model of skeletal muscle regeneration. *Mathematical Methods in the Applied Sciences* **41**:8589–8602. DOI: https://doi.org/10.1002/mma.4908

Swat MH, Thomas GL, Belmonte JM, Shirinifard A, Hmeljak D, Glazier JA. 2012. Multi-scale modeling of tissues using CompuCell3D. *Methods in Cell Biology* **110**:325–366. DOI: https://doi.org/10.1016/B978-0-12-388403-9.00013-8, PMID: 22482955

Tatsumi R, Anderson JE, Nevoret CJ, Halevy O, Allen RE. 1998. HGF/SF is present in normal adult skeletal muscle and is capable of activating satellite cells. *Developmental Biology* **194**:114–128. DOI: https://doi.org/10.1006/dbio.1997.8803, PMID: 9473336

Teixeira CFP, Zamunér SR, Zuliani JP, Fernandes CM, Cruz-Hofling MA, Fernandes I, Chaves F, Gutiérrez JM. 2003. Neutrophils do not contribute to local tissue damage, but play a key role in skeletal muscle regeneration, in mice injected with *Bothrops asper* snake venom. *Muscle & Nerve* **28**:449–459. DOI: https://doi.org/10.1002/mus.10453

Ten Broek RW, Grefte S, Von den Hoff JW. 2010. Regulatory factors and cell populations involved in skeletal muscle regeneration. *Journal of Cellular Physiology* **224**:7–16. DOI: https://doi.org/10.1002/jcp.22127, PMID: 20232319

Tigner A, Ibrahim SA, Histology MI. 2021. Histology, white blood cell. https://www.ncbi.nlm.nih.gov/books/NBK563148/ [Accessed May 16, 2022].

Torrente Y, Fahime EE, Caron NJ, Del Bo R, Belicchi M, Pisati F, Tremblay JP, Bresolin N. 2003. Tumor necrosis factor-α (TNF-α) stimulates chemotactic response in mouse myogenic cells. *Cell Transplantation* **12**:91–100. DOI: https://doi.org/10.3727/000000003783985115

Uribe-Querol E, Rosales C. 2020. Phagocytosis: our current understanding of a universal biological process. *Frontiers in Immunology* **11**:1066. DOI: https://doi.org/10.3389/fimmu.2020.01066, PMID: 32582172

Valle X. 2011. Clinical practice guide for muscular injuries: epidemiology, diagnosis, treatment and prevention. *British Journal of Sports Medicine* **45**:e2. DOI: https://doi.org/10.1136/bjsm.2010.081570.20

van de Kamp J, Jahnen-Dechent W, Rath B, Knuechel R, Neuss S. 2013. Hepatocyte growth factor-loaded biomaterials for mesenchymal stem cell recruitment. *Stem Cells International* **2013**:1–9. DOI: https://doi.org/10.1155/2013/892065

van den Bos E, Walbaum S, Horsthemke M, Bachg AC, Hanley PJ. 2020. Time-lapse imaging of mouse macrophage chemotaxis. *Journal of Visualized Experiments* **01**:60750. DOI: https://doi.org/10.3791/60750

Virgilio KM, Martin KS, Peirce SM, Blemker SS. 2018. Agent-based model illustrates the role of the microenvironment in regeneration in healthy and mdx skeletal muscle. *Journal of Applied Physiology* **125**:1424–1439. DOI: https://doi.org/10.1152/japplphysiol.00379.2018, PMID: 30070607

Virgilio KM, Jones BK, Miller EY, Ghajar-Rahimi E, Martin KS, Peirce SM, Blemker SS. 2021. Computational models provide insight into in vivo studies and reveal the complex role of fibrosis in mdx muscle regeneration. *Annals of Biomedical Engineering* **49**:536–547. DOI: https://doi.org/10.1007/s10439-020-02566-1

Vogel DYS, Heijnen PDAM, Breur M, de Vries HE, Tool ATJ, Amor S, Dijkstra CD. 2014. Macrophages migrate in an activation-dependent manner to chemokines involved in neuroinflammation. *Journal of Neuroinflammation* **11**:23. DOI: https://doi.org/10.1186/1742-2094-11-23, PMID: 24485070

Wagatsuma A. 2007. Endogenous expression of angiogenesis-related factors in response to muscle injury. *Molecular and Cellular Biochemistry* **298**:151–159. DOI: https://doi.org/10.1007/s11010-006-9361-x, PMID: 17435971

Waldemer-Streyer RJ, Kim D, Chen J. 2022. Muscle cell-derived cytokines in skeletal muscle regeneration. *The FEBS Journal* **289**:6463–6483. DOI: https://doi.org/10.1111/febs.16372, PMID: 35073461

Wang W, Pan H, Murray K, Jefferson BS, Li Y. 2009. Matrix metalloproteinase-1 promotes muscle cell migration and differentiation. *The American Journal of Pathology* **174**:541–549. DOI: https://doi.org/10.2353/ajpath.2009.080509, PMID: 19147819

Wang YX, Dumont NA, Rudnicki MA. 2014. Muscle stem cells at a glance. *Journal of Cell Science* **127**:4543–4548. DOI: https://doi.org/10.1242/jcs.151209, PMID: 25300792

Wang J. 2018. Neutrophils in tissue injury and repair. *Cell and Tissue Research* **371**:531–539. DOI: https://doi.org/10.1007/s00441-017-2785-7, PMID: 29383445

Wang X, Zhao W, Ransohoff RM, Zhou L. 2018. Infiltrating macrophages are broadly activated at the early stage to support acute skeletal muscle injury repair. *Journal of Neuroimmunology* **317**:55–66. DOI: https://doi.org/10.1016/j.jneuroim.2018.01.004, PMID: 29325905

Wang X, Hossain M, Bogoslowski A, Kubes P, Irimia D. 2020. Chemotaxing neutrophils enter alternate branches at capillary bifurcations. *Nature Communications* **11**:1–12. DOI: https://doi.org/10.1038/s41467-020-15476-6

Watanabe S, Alexander M, Misharin AV, Budinger GRS. 2019. The role of macrophages in the resolution of inflammation. *The Journal of Clinical Investigation* **129**:2619–2628. DOI: https://doi.org/10.1172/JCI124615, PMID: 31107246

Westman AM, Peirce SM, Christ GJ, Blemker SS, ed. 2021. Agent-based model provides insight into the mechanisms behind failed regeneration following volumetric muscle loss injury. *PLOS Computational Biology* **17**:e1008937. DOI: https://doi.org/10.1371/journal.pcbi.1008937

Wickler SJ. 1981. Capillary supply of skeletal muscles from acclimatized white-footed mice Peromyscus. *The American Journal of Physiology* **241**:R357–R361. DOI: https://doi.org/10.1152/ajpregu.1981.241.5.R357, PMID: 7304781

Wipff PJ, Rifkin DB, Meister JJ, Hinz B. 2007. Myofibroblast contraction activates latent TGF-beta1 from the extracellular matrix. *The Journal of Cell Biology* **179**:1311–1323. DOI: https://doi.org/10.1083/jcb.200704042, PMID: 18086923

Yennek S, Burute M, Théry M, Tajbakhsh S. 2014. Cell adhesion geometry regulates non-random DNA segregation and asymmetric cell fates in mouse skeletal muscle stem cells. *Cell Reports* **7**:961–970. DOI: https://doi.org/10.1016/j.celrep.2014.04.016, PMID: 24836002

Yin H, Price F, Rudnicki MA. 2013. Satellite cells and the muscle stem cell niche. *Physiological Reviews* **93**:23–67. DOI: https://doi.org/10.1152/physrev.00043.2011, PMID: 23303905

Yokoyama T, Sekiguchi K, Tanaka T, Tomaru K, Arai M, Suzuki T, Nagai R. 1999. Angiotensin II and mechanical stretch induce production of tumor necrosis factor in cardiac fibroblasts. *The American Journal of Physiology* **276**:H1968–H1976. DOI: https://doi.org/10.1152/ajpheart.1999.276.6.H1968, PMID: 10362677

Yoon YS, Lee YJ, Choi YH, Park YM, Kang JL. 2016. Macrophages programmed by apoptotic cells inhibit epithelial-mesenchymal transition in lung alveolar epithelial cells via PGE2, PGD2, and HGF. *Scientific Reports* **6**:1–18. DOI: https://doi.org/10.1038/srep20992

You JS, Barai P, Chen J. 2023. Sex differences in skeletal muscle size, function, and myosin heavy chain isoform expression during post-injury regeneration in mice. *Physiological Reports* **11**:e15791. DOI: https://doi.org/10.14814/phy2.15791, PMID: 37620103

Zhao W, Zhao H, Li M, Huang C. 2020. Microfluidic devices for neutrophil chemotaxis studies. *Journal of Translational Medicine* **18**:168. DOI: https://doi.org/10.1186/s12967-020-02335-7, PMID: 32293474

Zimowska M, Olszynski KH, Swierczynska M, Streminska W, Ciemerych MA. 2012. Decrease of MMP-9 activity improves soleus muscle regeneration. *Tissue Engineering. Part A* **18**:1183–1192. DOI: https://doi.org/10.1089/ten.TEA.2011.0459, PMID: 22429194

Zou Y, Zhang RZ, Sabatelli P, Chu ML, Bönnemann CG. 2008. Muscle interstitial fibroblasts are the main source of collagen VI synthesis in skeletal muscle: implications for congenital muscular dystrophy types Ullrich and Bethlem. *Journal of Neuropathology and Experimental Neurology* **67**:144–154. DOI: https://doi.org/10.1097/nen.0b013e3181634ef7, PMID: 18219255